

# Estimation of Physical Conditions in the Cold Phase of the Interstellar Medium in the sub-DLA System at $z = 2.06$ in the Spectrum of the Quasar J 2123–0050

V.V. Klimenko<sup>1,2\*</sup>, S.A. Balashev<sup>1,2</sup>, A.V. Ivanchik<sup>1,2</sup>, D.A. Varshalovich<sup>1,2</sup>

<sup>1</sup>*Ioffe Physicotechnical Institute, Russian Academy of Sciences, ul. Politekhnicheskaya 26, St. Petersburg, 194021 Russia*

<sup>2</sup>*St. Peter the Great St. Petersburg Polytechnic University, Polytechnicheskaya ul. 29, St. Petersburg, 195251 Russia Received October 21, 2015*

Received 21 October, 2015

## Abstract

An independent analysis of the molecular hydrogen absorption system at redshift  $z_{\text{abs}} = 2.059$  in the spectrum of the quasar J 2123–0050 is presented. The  $\text{H}_2$  system consists of two components (A and B) with column densities  $\log N_{\text{H}_2}^{\text{A}} = 17.94 \pm 0.01$  and  $\log N_{\text{H}_2}^{\text{B}} = 15.16 \pm 0.02$ . The spectrum exhibits the lines of HD molecules ( $\log N_{\text{HD}}^{\text{A}} = 13.87 \pm 0.06$ ) and the neutral species C I and C I associated with the  $\text{H}_2$  absorption system. For the molecular hydrogen lines near the quasar's Ly $\beta$  and O VI emission lines, we detect a nonzero residual flux,  $\sim 3\%$  of the total flux, caused by the effect of partial coverage of the quasar's broad-line region by an  $\text{H}_2$  cloud. Due to the smallness of the residual flux, the effect does not affect the  $\text{H}_2$  column density being determined but increases the statistics of observations of the partial coverage effect to four cases. The uniqueness of the system being investigated is manifested in a high abundance of the neutral species  $\text{H}_2$  and C I at the lowest H I column density,  $\log N_{\text{HI}} = 19.18 \pm 0.15$ , among the high redshift systems. The  $\text{H}_2$  and C I column densities in the system being investigated turn out to be higher than those in similar systems in our Galaxy and the Magellanic Clouds by two or three orders of magnitude. The  $N_{\text{HD}}/2N_{\text{H}_2}$  ratio for component A has turned out to be also unusually high,  $(4.26 \pm 0.60) \times 10^{-5}$ , which exceeds the deuterium abundance (D/H) for high-redshift systems by a factor of 1.5. Using the H I,  $\text{H}_2$ , HD, and C I column densities and the populations of excited  $\text{H}_2$  and C I levels, we have investigated the physical conditions in components A and B. Component A represents the optically thick case; the gas has a low number density ( $n \approx 30 \text{ cm}^{-3}$ ) and a temperature  $T \sim 140 \text{ K}$ . In component B, the medium is optically thin with  $n < 100 \text{ cm}^{-3}$  and  $T \geq 100 \text{ K}$ . The ultraviolet (UV) background intensity in the clouds exceeds the mean intensity in our Galaxy by almost an order of magnitude. A high gas ionization fraction,  $n_{\text{H}^+}/n_{\text{H}} \sim 10^{-2}$ , which can be the result of partial shielding of the system from hard UV radiation, is needed to describe the high HD and C I column densities. Using our simulations with the PDR Meudon code, we can reconstruct the observed column densities of the species within the model with a constant density ( $n_{\text{H}} \sim 40 \text{ cm}^{-3}$ ). A high  $\text{H}_2$  formation rate (higher than the mean Galactic value by a factor of 10–40) and high gas ionization fraction and UV background intensity are needed in this case.

**Key words.** galaxies, interstellar medium, absorption systems, quasar J 2123–0050

## 1. Introduction

One way to study the physical conditions and chemical composition of the interstellar and intergalactic media at high redshifts is to investigate the absorption systems in the spectra of bright extragalactic sources, such as quasars or gamma-ray bursts. Most of the absorption lines in the spectra of such objects are associated with the Lyman alpha (Ly $\alpha$ ) lines of neutral hydrogen falling within the optical range due to the cosmological redshift  $z$ . The absorption systems of the Ly $\alpha$  forest are believed to relate to the clouds of almost fully ionized hydrogen located in the intergalactic medium on the line of sight between the quasar and the observer. Neutral hydrogen absorption systems with a very high H I column density ( $\log N_{\text{HI}} > 19$ , here and below, the column densities are measured in  $\text{cm}^{-2}$ ) are detected approxi-

mately in 10 % of the quasar spectra. If the column density  $\log N_{\text{HI}} > 20.3$ , then such an absorption system is called a DLA system (Damped Lyman Alpha system); if  $19.0 < \log N_{\text{HI}} < 20.3$ , then the system belongs to the class of sub-DLA systems. The DLA systems are believed to be the main reservoirs of neutral hydrogen in the early Universe [1, 2]. In the spectra of quasars, the sub-DLA and DLA systems are identified owing to the broad Ly $\alpha$  absorption line with characteristic Lorentz wings. Another peculiarity of such systems is the presence of many absorption lines of heavy elements<sup>1</sup> in the spectrum at the same redshift. The DLA systems appear to be the disks or halos of protogalaxies with a radius of several 10 kpc [3]. Due to the high column density  $N_{\text{HI}}$ , the matter in DLA systems is shielded from ionizing ultraviolet (UV) radiation with an energy exceeding the

\* E-mail: slava.klimenko@gmail.com

<sup>1</sup> Elements heavier than helium are called metals.

ionization energy of the hydrogen,  $E > 13.6$  eV. But, at the same time, it is believed that the medium in sub-DLA systems can be partially shielded due to the lower HI column density, and gas regions with different ionization fractions can simultaneously fall on the line of sight. When the elemental abundances in sub-DLA systems are analyzed, the ionization corrections should be applied (see, e.g., [4, 5]).

The detection of the  $\text{H}_2$ , HD, and CO molecular absorption systems (see [6, 7, 8, 9]), which are known from observations in our Galaxy and Local Group galaxies (see, e.g., [10, 11, 12]) relate to dense cold clouds ( $n \sim 10 - 500 \text{ cm}^{-3}$ ,  $T \sim 40 - 200 \text{ K}$ ) in the interstellar medium, suggests that the matter in DLA and sub-DLA systems belongs to the interstellar medium and not to the intergalactic one.

The  $\text{H}_2$  absorption systems are observed in less than 10% of the spectra containing DLA and sub-DLA systems [18, 19, 20]. Spectra with a high signal-to-noise ratio ( $S/N > 10$ ) and a high spectral resolution ( $R \sim 20\,000 - 110\,000$ ), which is a limiting problem for the largest optical telescopes at present, are needed for their investigation. Thirty high-redshift systems have been detected (see, e.g., [9, 13]) since the first identification of  $\text{H}_2$  molecular lines in the spectra of quasars [6], despite the fact that more than 12 000 DLA systems are already known [2]. We have developed a technique of searching for  $\text{H}_2$  candidates in the medium-resolution spectra of the Sloan Digital Sky Survey (SDSS, [21]), which has revealed more than 50  $\text{H}_2$  candidates to date [19]. Moreover, the first observations of eight candidates at the Very Large Telescope (VLT) led to their confirmation (Balashev et al., in preparation). The main objective of studying high-redshift molecular hydrogen clouds is to determine the physical conditions in the cold phase of the interstellar medium. This is important for understanding the star formation and evolution of galaxies at high redshifts and for understanding the nature of DLA systems and their connection with galaxies.

In this paper, we present an independent analysis of the  $\text{H}_2$ /HD absorption system at redshift  $z_{\text{abs}} = 2.059$  in the VLT spectrum of the quasar J 2123–0050. Previously, this system has already been investigated in the quasar spectrum taken at the Keck telescope. However, the results of two papers [22, 23] disagree both in the number of components of the investigated absorption system and in the estimated  $\text{H}_2$  column density. A high signal-to-noise ratio in continuum in the VLT spectrum,  $S/N \sim 20 - 120$ , compared to  $S/N \sim 10 - 40$  in the Keck spectrum allowed one to study in more detail the structure of this system and to obtain more accurate column densities of  $\text{H}_2$  and HD molecules at various rotational levels.

An unusual feature of the  $\text{H}_2$  system in the spectrum of J 2123–0050 is a high  $\text{H}_2$  column density for one of the components of the absorption system,  $\log N_{\text{H}_2}^{\text{A}} = 17.94 \pm 0.01$ , despite the fact that the atomic hydrogen column density  $\log N_{\text{HI}} = 19.18 \pm 0.15$  [5] is lowest among the DLA and sub-DLA systems in which the  $\text{H}_2$  systems were detected (see Fig. 1). The measured  $\text{H}_2$  column density in the spectrum of J 2123–0050 is almost three orders of magnitude higher than that for the  $\text{H}_2$  clouds located in our Galaxy and having similar column densities  $N_{\text{HI}}$ . One would think that such a difference

can be explained by a relatively low UV background intensity. However, it has been found that the UV background intensity in the sub-DLA system of J 2123–0050 to be considerably higher than the mean Galactic value, [5], [24].

Apart from the  $\text{H}_2$  molecules, the lines of HD molecules are detected in the system J 2123–0050 [23]. The  $N_{\text{HD}}/2N_{\text{H}_2}$  ratio in this system turned out to be a factor of 1.5 higher than the primordial deuterium abundance and a factor of 3 or 4 higher than the values measured in high redshift  $\text{H}_2$ /HD systems (see [9]). These and other facts are of additional interest for the studies of physical conditions in this  $\text{H}_2$  system.

## 2. OBSERVATIONAL DATA

The quasar J 2123–0050 (with redshift  $z_{\text{em}} = 2.261$  and apparent magnitude  $m_V = 16.6$ ) was identified in the SDSS. High-resolution spectra of this quasar were taken independently at the two largest optical telescopes, Keck (using the High Resolution Echelle Spectrograph, HIRES) and VLT (using the Ultraviolet and Visible Echelle Spectrograph, UVES). The quasar was observed at the Keck telescope in the wavelength range  $3071 - 5869 \text{ \AA}$  in 2006 under the U080Hb program (Prochaska). The data are in free access from the Keck archive<sup>2</sup>. The slit size was chosen to be  $0.4''$ , the CCD pixels were binned  $2 \times 1$ . These settings allowed a spectrum with a resolution  $R \sim 100\,000$  to be achieved. We reduced and added the exposures using the MAKEE software package<sup>3</sup>. The total exposure time was  $\sim 6.1 \text{ h}$ . J 2123–0050 was observed at the VLT in 2008 under the 81.A-0242 program (Ubachs). The data are in free access from the European Southern Observatory (ESO) archive<sup>4</sup>. Different settings were used for the blue and red arms of the UVES spectrograph. For the blue arm, the slit size was chosen to be  $0.8''$ , and the CCD pixels were binned  $2 \times 2$ . For the red arm, the slit size was chosen to be  $0.7''$ , and the CCD pixels were binned  $1 \times 1$ . These settings allow a spectrum with a resolution of 49 620 for the blue part and 56 990 for the red one to be achieved. We reduced the individual exposures using the UVES Common Pipeline Library (CPL) data reduction pipeline release 4.9.5 software package<sup>4</sup>. The total exposure time was  $\sim 11.3 \text{ h}$ .

## 3. THE SUB-DLA ABSORPTION SYSTEM AT $z = 2.06$

The sub-DLA system at redshift  $z_{\text{abs}} = 2.06$  in the spectrum of the quasar J 2123–0050 was first investigated by [5] and then by [24]. The sub-DLA system consists of at least two components with column densities  $\log N_{\text{HI}}(z = 2.05684) = 18.40 \pm 0.30$  and  $\log N_{\text{HI}}(z = 2.05930) = 19.18 \pm 0.15$  [5]. The lines of  $\text{H}_2$ , HD, C I, and Cl I molecules, which are known to be indicators of the cold phase of the interstellar medium (see, e.g., [25, 26, 27]), are detected in the component at  $z = 2.05930$ .

<sup>2</sup> <https://koa.ipac.caltech.edu/cgi-bin/KOA/nph-KOAllogin>

<sup>3</sup> <http://www.astro.caltech.edu/tb/makee>

<sup>4</sup> <ftp://ftp.eso.org/pub/dfs/pipelines/uves/uves-pipelinemanual-22.8.pdf>

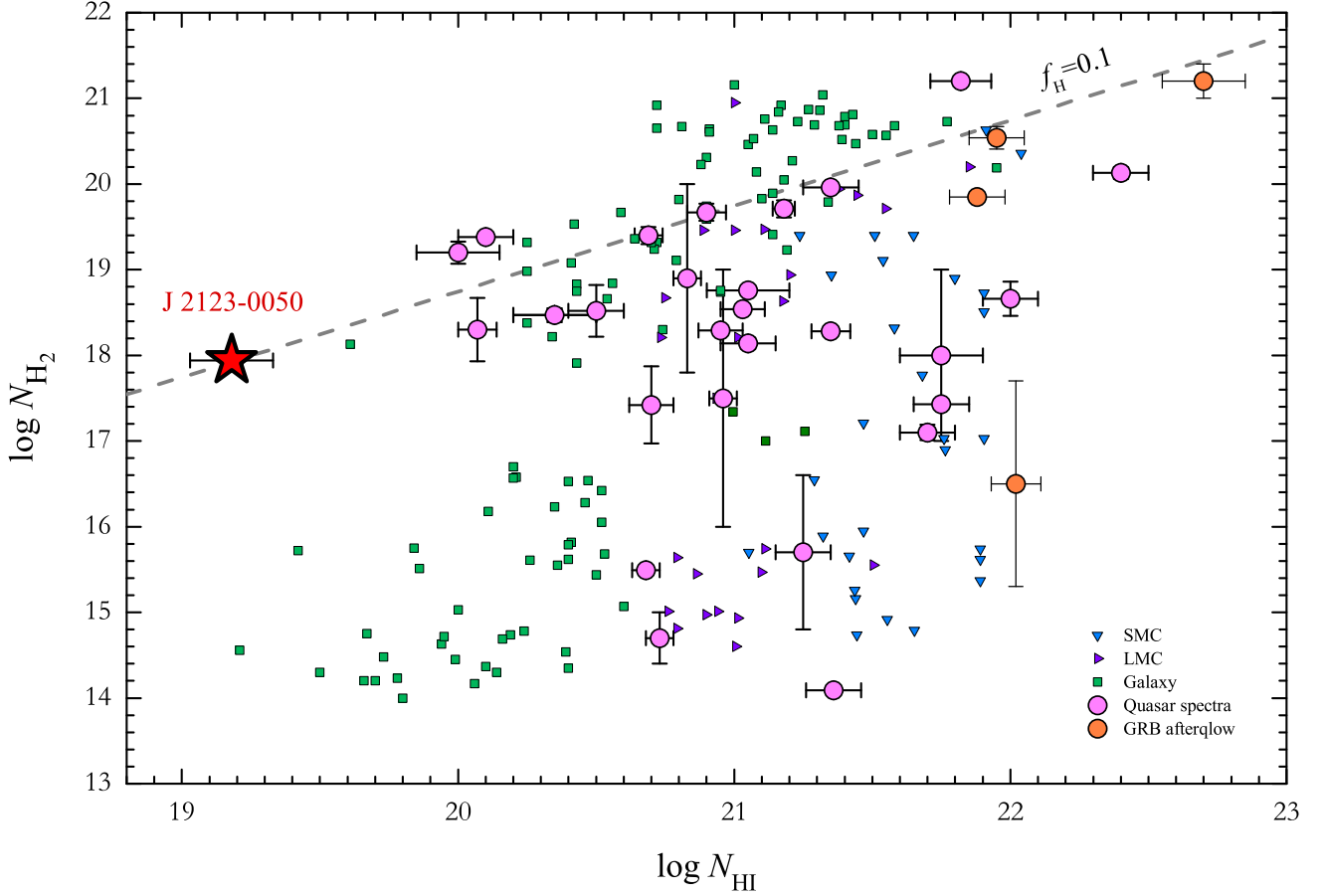


**Figure 1.** Measured  $\text{H}_2$  and  $\text{H I}$  column densities for the high-redshift DLA and sub-DLA systems identified in the spectra of quasars (filled dark circles – see, e.g., [9, 13]) and the spectra of GRB afterglows (filled light circles – see [1, 14, 15, 16]) as well as for the systems in our Galaxy and the Magellanic Clouds (squares, diamonds, and triangles – [12, 17]). The system being investigated has the lowest  $\text{H I}$  column density ( $\log N_{\text{H I}} = 19.18 \pm 0.15$ ) among the high-redshift systems with  $\log N_{\text{H}_2} \sim 18$ .

### 3.1. The Ionization Structure

It is well known that in contrast to DLA systems, where the medium is thought to be predominantly neutral, much of the hydrogen (up to 90%) in sub-DLA systems is in an ionized state, which should be taken into account when analyzing such systems. The sub-DLA systems are believed to have a layered (multiphase) structure. The hydrogen ionization fractions in the neutral and ionized phases are close to 0 and 1, respectively, i.e., the matter is separated into predominantly fully neutral and fully ionized phases and is not a mixture with some ionization fraction.

The metals in sub-DLA systems occupy a spatially larger region than does the neutral hydrogen; therefore, the structures of sub-DLA systems ( $\text{H I} + \text{H II}$ ) manifest themselves in the absorption lines of metals with different ionization states, such as O, S, Si, Al, Zn, etc. In a predominantly neutral medium, the metals are in the ground state, at the first ionization level with an energy above 13.6 eV, because the UV photons capable of ionizing such ions are absorbed by neutral hydrogen. In the region of almost fully ionized hydrogen in sub-DLA systems, the relationship between the number densities of metals at various ionization levels is established in

accordance with the balance between the recombination and ionization rates of the species. In the spectrum, such an ionization structure manifests itself in the simultaneous presence of absorption lines of metals with various ionization states in the same velocity components.

In the sub-DLA system in the spectrum of J 2123–0050, for example, Si is represented at least in three ionization states, Si II, Si III, and Si IV, whose absorption structure is shown in Fig. 2. The system has up to 20 individual components detected simultaneously in Si (and Al) lines in various ionization states. Given the ionization corrections, the metallicity changes from  $[\text{Si}/\text{H}] = +0.00 \pm 0.02^5$  to  $[\text{Si}/\text{H}] = -0.71 \pm 0.15$  [5].

## 4. THE MOLECULAR HYDROGEN SYSTEM

The  $\text{H}_2$  system in the spectrum of the quasar J 2123–0050 has been investigated in several studies. The lines of  $\text{H}_2$  and HD molecules were studied independently by [22] in the Keck spectrum and by [28] in

<sup>5</sup>  $[\text{X}/\text{H}] = \log(N(\text{X})/N(\text{H})) - \log(N(\text{X})/N(\text{H}))_{\odot}$  is the difference between the logarithms of the elemental abundance in the system being investigated and with respect to the abundance measured in the Solar system.

the VLT spectrum to place constraints on the possible time variation of the proton-to-electron mass ratio. The HD/2H<sub>2</sub> ratio of the molecular cloud was investigated by [23] in the Keck spectrum (for a comparison of the results of these analyses, see Table 1). We performed an independent analysis of this absorption system in the VLT spectrum. The parameters of the absorption system were determined by comparing the observed spectrum with the synthetic one. To determine the best-fit parameters, we used the Markov Chain Monte Carlo (MCMC) technique.

#### 4.1. Analysis of the H<sub>2</sub> System in the VLT Spectrum

The H<sub>2</sub> lines of nine Lyman bands and one Werner band fall within the wavelength range of the UVES spectrograph ( $3000 \text{ \AA} < \lambda < 11\,000 \text{ \AA}$ )<sup>6</sup>. At least two components (hereafter A and B) at redshifts  $z_A = 2.05932(5)$  and  $z_B = 2.05955(3)$  are detected in the H<sub>2</sub> lines of the transitions from the rotational levels  $J = 0$  to  $J = 5$ . The relative velocity shift between components A and B is fairly large compared to the width of the UVES point spread function  $\sim 6 \text{ km s}^{-1}$  and the Doppler line broadening  $\sim 1 - 5 \text{ km s}^{-1}$  and is  $\sim 22 \text{ km s}^{-1}$ . Therefore, the individual components in the transition lines profiles are resolvable even for the saturated  $J = 0$  and 1 levels. Since no evidence for the presence of additional components was found (see Fig. 3), we used a two-component model. The best-fit parameters and their errors are given in Table 2. The synthetic spectrum of the H<sub>2</sub> absorption system is shown in Fig. 4. The total column densities are  $\log N_{\text{H}_2}^A = 17.94 \pm 0.01$  and  $\log N_{\text{H}_2}^B = 15.16 \pm 0.02$ . Note that the Doppler parameter  $b_J$  increases with increasing level  $J$ . This effect is well known for H<sub>2</sub> systems [29, 30, 31] and can be caused by a nonuniform distribution of H<sub>2</sub> molecules at different rotational levels  $J$  over the molecular cloud volume (for more details, see [32]).

In Fig. 5 the relative rotational level populations  $N_J/g_J$  are plotted against the level excitation energy  $E_J$  ( $g_J$  is the statistical weight of level  $J$ ) for the two components of the H<sub>2</sub> system. For the component A, the  $J = 0$  and 1 levels are populated through collisions. The kinetic temperature of the gas determined from the ratio of the ortho- and para-hydrogen column densities is  $T_A = 139 \pm 6 \text{ K}$ . The  $J = 3, 4$ , and 5 levels are populated mainly through radiative pumping. In J 2123–0050 B, the total H<sub>2</sub> column density is lower than that in component A by almost three orders of magnitude. In an optically thin medium, the radiative pumping process is important for all H<sub>2</sub> levels; therefore, the temperature determined from the ratio of the ortho- and para-hydrogen column densities,  $T_B = 648 \pm 126 \text{ K}$ , can differ significantly from the kinetic temperature of the gas.

#### 4.2. The Residual Flux in Molecular Hydrogen Lines

For H<sub>2</sub> clouds at high redshifts, the partial coverage effect, when the H<sub>2</sub> cloud partially covers the quasar’s emission regions, is possible (see, e.g., [33, 31, 34]). Part of the quasar’s emission passes by the absorption cloud and produces a residual flux (RF) in the spectrum at the bottom of the H<sub>2</sub> absorption lines. Disregarding this

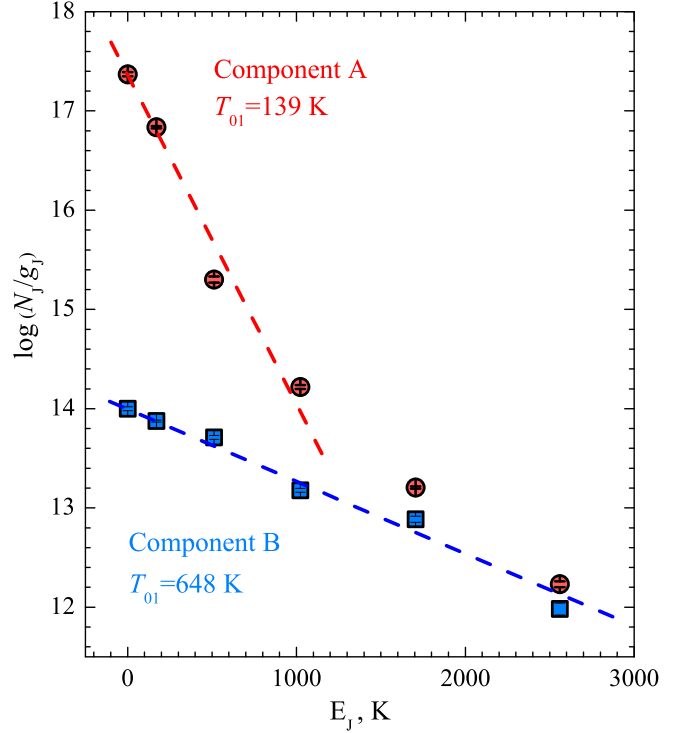


**Figure 5.** Populations  $N_J$  of H<sub>2</sub> rotational levels normalized to the statistical weight  $g_J$  versus level excitation energy  $E_J$ . The circles and squares correspond to components A and B of the H<sub>2</sub> absorption system. The straight lines correspond to the excitation temperatures  $T_{01}$  determined from the relative populations of the  $J = 0$  and 1 levels.

effect in the analysis of H<sub>2</sub> lines can lead to an underestimation of the H<sub>2</sub> column density (by up to two orders of magnitude). As it was shown by [35] the effect of partial coverage of quasars by H<sub>2</sub> absorption systems at high redshifts should be observed at least in 10 % of the cases.

In the spectrum of J 2123–0050, we detect a nonzero RF for component A (in the most saturated H<sub>2</sub> lines of the transitions from  $J = 0, 1$ ) in the region of the Ly $\beta$  and O VI emission lines,  $3.4 \pm 0.5\%$  of the continuum flux. Figure 6 shows the line positions in the spectrum (upper left panel) and the RF at the line minimum (lower left panel). Analysis of the dependence of the RF on the product of the wavelength and oscillator strength for the H<sub>2</sub> transitions (for more details, see [34]) suggests that a nonzero RF in the H<sub>2</sub> line is most likely not caused by the convolution of the saturated lines with the instrumental function of the spectrograph but is probably a consequence of the partial coverage effect (see the right panel in Fig. 6). To analyze the H<sub>2</sub> absorption system, we used four models: (i) without any sources of additional radiation, (ii) with a source of additional radiation in continuum, (iii) with a source of additional radiation in emission lines, and (iv) with two sources of additional radiation in continuum and emission lines. For a quantitative comparison, we used the statistical Akaike (corrected Akaike information criterion; see [36])

<sup>6</sup> <http://www.eso.org/sci/facilities/paranal/instruments/uves/Akaike>

**Table 1.** Comparison of the measured H<sub>2</sub> and HD column densities in component A of the H<sub>2</sub> absorption system at  $z_{\text{abs}} = 2.059$  in the spectrum of J 2123–0050.

No.	$z_A$	$\log N_A(\text{H}_2)$	$\log N_A(\text{HD})$	$T_{01}, \text{K}$	$\text{HD}/2\text{H}_2$
[22]	2.0593276(5)	$15.76 \pm 0.03$	$12.95 \pm 0.03$	$116 \pm 17$	$(7.7 \pm 0.8) \times 10^{-4}$
	2.0593290(4)	$17.55 \pm 0.04$	$13.69 \pm 0.05$	$-97 \pm 51$	$(6.9 \pm 1.0) \times 10^{-5}$
[23]	2.0594(1)	$17.64 \pm 0.15$	$13.84 \pm 0.20$	$281^{+2700}_{-134}$	$(7.9 \pm 4.6) \times 10^{-5}$
This work	2.0593245(5)	$17.94 \pm 0.01$	$13.87 \pm 0.06$	$138.6 \pm 5.8$	$(4.3 \pm 0.6) \times 10^{-5}$

**Table 2.** Results of our analysis of the H<sub>2</sub> absorption system in the spectrum of J 2123–0050 in the sub-DLA system at  $z_{\text{abs}} = 2.059$ .

Component A $z_A = 2.0593245$				Component B $z_B = 2.0595532$			
	J	$\log N_A$	$b_A, \hat{e}/\hat{n}$		J	$\log N_B$	$b_B, \hat{e}/\hat{n}$
H <sub>2</sub>	0	$17.37 \pm 0.02$	$1.71 \pm 0.04$	H <sub>2</sub>	0	$14.00 \pm 0.02$	$5.18 \pm 0.51$
	1	$17.79 \pm 0.01$	$2.07 \pm 0.05$		1	$14.84 \pm 0.01$	$5.24 \pm 0.11$
	2	$16.00 \pm 0.03$	$2.97 \pm 0.05$		2	$14.41 \pm 0.01$	$5.02 \pm 0.18$
	3	$15.54 \pm 0.02$	$3.56 \pm 0.06$		3	$14.50 \pm 0.01$	$4.71 \pm 0.30$
	4	$14.16 \pm 0.01$	$4.64 \pm 0.23$		4	$13.84 \pm 0.03$	$7.86 \pm 0.57$
	5	$13.75 \pm 0.03$	$5.10 \pm 0.51$		5	$13.50 \pm 0.06$	$7.36 \pm 0.80$
	$\Sigma_J$	$17.94 \pm 0.01$			$\Sigma_J$	$15.16 \pm 0.02$	
HD	0	$13.87 \pm 0.06$	$2.0 \pm 0.6$	HD	0	not detected	
HD/2H <sub>2</sub>		$(4.26 \pm 0.60) \times 10^{-5}$		HD/2H <sub>2</sub>			

criterion<sup>7</sup>. The results of our analysis are presented in Table 3. For models (iii) and (iv), the AICC values are found to be lower ( $\Delta\text{AICC} \sim -40$ ) than those for models (i) and (ii). Taking into account the RF in continuum allows the AICC values to be reduced by 10 more units. The H<sub>2</sub> lines are best described by model (iv). It should be noted that in view of the low H<sub>2</sub> column density and the RF smallness (about 1–4 %), allowance for the partial coverage effect affects weakly the H<sub>2</sub> column densities being determined (see columns 7 and 8 in Table 3). However, this case increases the statistics of observations of the partial coverage effect for high-redshift H<sub>2</sub> absorption systems to four cases.

## 5. ANALYSIS OF HD LINES

To estimate the column density of HD molecules, we used the VLT spectrum. Because of the smallness of the H<sub>2</sub> column density in component B ( $\log N_{\text{H}_2}^B = 15.16 \pm 0.02$ ), the expected column density of HD molecules does not exceed  $\log N_{\text{HD}}^B \leq 11$ ; therefore, it is impossible to detect the HD lines in this component at the existing sensitivity level of modern telescopes. The lines of HD molecules are detected only in component A for the transitions of the Lyman and Werner bands up to L8-0 and W0-0. To determine the HD column density ( $J = 0$ ), we used the L0-0, L2-0, L3-0, L5-0, L7-0, and L8-0 transition lines of HD molecules, which

do not overlap with the Ly $\alpha$ -forest lines. The laboratory wavelengths of the HD transitions were taken from [38]. The oscillator strengths were taken from the calculations by [39]. The estimated column density of HD molecules is  $\log N_{\text{HD}}^A = 13.87 \pm 0.06$ . The HD line profiles and the fitted synthetic spectrum are shown in Fig. 7. The derived value is consistent with the estimate  $\log N_{\text{HD}}^A = 13.84 \pm 0.20$  [23]. However, owing to the higher signal-to-noise ratio in the VLT spectrum, our estimate of  $N_{\text{HD}}$  is considerably more accurate.

## 6. NEUTRAL CARBON

The structure of the neutral carbon line for the transitions from the ground,  $2s^2 2p^2 {}^3P_0$  (C I), and two excited,  $2s^2 2p^2 {}^3P_1$  (C I\*) and  $2s^2 2p^2 {}^3P_2$  (C I\*\*), states consists of at least two components at redshifts coincident with the positions of components A and B of the H<sub>2</sub> system. The neutral carbon lines were analyzed for four models. Model (i) consists of two C I components associated with components A and B of the H<sub>2</sub> absorption system. In comparison with model (i), an additional component with a considerably larger Doppler parameter is used in model (ii). Models (iii) and (iv) differ from models (i) and (ii) by allowance for the RF for the C I lines falling into the C IV emission line wing (for more details, see Section 6.1). The results of our analysis are presented in Table 4.

Model (i) describes the C I line profiles for the transitions from the ground state for component A not well enough ( $\chi_{\text{red}}^2 \approx 1.5$ ). Model (ii) gives a considerably better description ( $\chi_{\text{red}}^2 \approx 0.9$ ) the change in the AICC value compared to model (i) is  $\Delta\text{AICC} = -264$ , which,

<sup>7</sup> The most preferred model is determined using the difference of the AICC values.  $\Delta\text{AICC} = 10$  is deemed to mean strong evidence for the model with the smaller AICC value [37].

**Table 3.** Comparison of the results of our analysis of the H<sub>2</sub> absorption system for various residual flux (RF) models. The columns present the following: 2 – the reduced  $\chi^2$  value; 3 – the absolute AICC value [36]; 4 – the difference of the AICC values; 5 and 6 – RF<sub>cont</sub> and RF<sub>emis</sub> – the RFs due to the effect of partial coverage of the quasar’s emission region in continuum and emission lines, respectively; 7 and 8 – the measured H<sub>2</sub> column densities in component A for the transitions from the J = 0 and 1 levels.

Model	$\chi^2_{red}$	AICC	$\Delta AICC$	RF <sub>cont</sub>	RF <sub>emis</sub>	$\log N_{H_2}^A(J=0)$	$\log N_{H_2}^A(J=1)$
i	1.11	374.7	0	no	no	$17.36 \pm 0.02$	$17.79 \pm 0.01$
ii	1.05	363.9	-10.8	$1.1 \pm 0.4$	no	$17.38 \pm 0.02$	$17.80 \pm 0.01$
iii	0.94	330.0	-44.7	no	$2.7 \pm 0.5$	$17.35 \pm 0.02$	$17.78 \pm 0.01$
iv	0.91	321.3	-53.4	$1.1 \pm 0.3$	$3.4 \pm 0.5$	$17.37 \pm 0.02$	$17.79 \pm 0.01$

**Table 4.** Comparison of the results of analysis of the C I lines in the spectrum of J 2123–0050 for four models. (i) and (ii) – without allowance for the RF in the C IV emission line, (iii) and (iv) – with allowance for the RF. The RF is measured in % of the total flux. The redshifts of the components are:  $z_A = 2.0593245(4)$ ,  $z_B = 2.059546(3)$ ,  $z_C = 2.059330(3)$ .

Model		$\log N_{CI}$	$\log N_{CI^*}$	$\log N_{CI^{**}}$	$b, \text{ km s}^{-1}$	RF	$\chi^2_{red}$	AICC
(i)	A	$13.82 \pm 0.02$	$13.26 \pm 0.02$	$12.65 \pm 0.02$	$1.31 \pm 0.03$	no	1.53	638
	B	$12.71 \pm 0.02$	$12.43 \pm 0.04$	$11.94 \pm 0.18$	$4.37 \pm 0.44$			
(ii)	A	$13.91 \pm 0.03$	$13.46 \pm 0.03$	$12.65 \pm 0.03$	$0.88 \pm 0.04$	no	0.91	386.4
	B	$12.71 \pm 0.02$	$12.43 \pm 0.03$	$11.90 \pm 0.09$	$4.18 \pm 0.27$			
	C	$12.78 \pm 0.03$	no	no	$6.89 \pm 0.60$			
(iii)	A	$13.84 \pm 0.03$	$13.27 \pm 0.02$	$12.63 \pm 0.04$	$1.32 \pm 0.04$	$1 \pm 1$	1.52	635
	B	$12.71 \pm 0.03$	$12.43 \pm 0.04$	$11.90 \pm 0.18$	$4.40 \pm 0.50$			
(iv)	A	$13.91 \pm 0.03$	$13.47 \pm 0.04$	$12.64 \pm 0.03$	$0.87 \pm 0.04$	$1 \pm 1$	0.91	388.4
	B	$12.71 \pm 0.02$	$12.43 \pm 0.03$	$11.85 \pm 0.13$	$4.25 \pm 0.27$			
	C	$12.78 \pm 0.03$	no	no	$7.26 \pm 0.70$			

according to the estimate by [37], is strong evidence for model (ii). Figure 8 shows the synthetic spectrum for model (ii) fitted into the quasar’s observed spectrum. The appearance of an additional C I subcomponent that is not detected in the H<sub>2</sub> lines can be explained by the presence of neutral carbon associated with the ionized part of the sub-DLA system.

According to the estimate by [5], up to 90 % of the matter in the sub-DLA system being investigated is in an ionized state. Assuming that the C<sup>+</sup> ions are distributed uniformly over the volume, the bulk of the C<sup>+</sup> column density belongs to the ionized gas, where the electron number density ( $n_e \sim n_{H^+}$ ) turns out to be three orders of magnitude higher than that in the neutral medium ( $n_e < 10^{-3} \times n_H$ ; see e.g., [40, 41]). As a result of these two factors, the amount of C I formed in the recombination reaction of C<sup>+</sup> ions with electrons can reach the observed value in component C:  $\log N_{CI} \sim 13$ . From the chemical equilibrium condition,

$$N_{CI} = N_{C^+} \frac{n_e \alpha(C^+)}{\beta(C)}, \quad (1)$$

where  $\alpha(C^+)$  is the recombination coefficient ( $\alpha(C^+) \sim 10^{-12} \text{ cm}^3 \text{ s}^{-1}$  for  $T \simeq 3 \times 10^3 \text{ K}$ , see [42]),  $\beta(C) = \chi_{UV} \times 2.1 \times 10^{-10} \text{ s}^{-1}$  – is the CI photoionization rate (see., e.g., [43]),  $\chi_{UV}$  is the UV background intensity with respect to the mean Galactic value [44]. However, since the C II 1334.5 Å absorption line in the spectrum consists of several overlapping saturated components,

the total C<sup>+</sup> column density cannot be determined. On the other hand, the amount of C<sup>+</sup> can be estimated by assuming that the carbon abundance with respect to its solar abundance is the same as that for sulfur (S). For metallicity  $[S/H] = -0.2$  and  $\log N_H^{\text{tot}} = 20.06$  [5], we obtain  $\log N_{C^+}^{\text{tot}} = 16.25$ . The fraction of C<sup>+</sup> ions associated with the ionized part of the sub-DLA system can be estimated as  $N_{C^+}^{\text{tot}} \times N_{H^+}/N_H^{\text{tot}} = 10^{16.2}$ . Then, according to Eq. (1), we obtain

$$N_{CI} = 0.8 \times 10^{13} \times \frac{n_e}{1 \text{ m}^{-3}} \times \frac{10}{\chi_{UV}} \text{ cm}^{-2}, \quad (2)$$

which is consistent with  $\log N_{CI}^C = 12.78$  for model (ii) from Table 4.

### 6.1. The Partial Coverage Effect for the Neutral Carbon System

The absorption lines of two transitions, C I 1328.8 Å and 1656.9 Å, shifted by the factor  $(1 + z_{\text{abs}})$  are in the region of the quasar N v C IV emission lines, respectively. Out of these C I lines, only the C I 1656.9 Å line falls within the wavelength range of the quasar’s VLT spectrum accessible to analysis. As was shown by [33], when analyzing the quasar Q 1232+082, the residual flux in the C I lines due to the partial coverage effect can reach 20 – 30 % of the total flux, which can change significantly the C I column densities being determined. To

check this possibility, we varied the residual flux in the C I lines near the C IV emission line, along with other parameters. The results of our analysis with (models (iii) and (iv)) and without (models (i) and (ii)) taking into account the RF are compared in Table 4. In models (ii) and (iv), the RF is detected at  $1 \pm 1\%$  of the total flux. However, since the C I lines are unsaturated, allowance for the RF in our analysis barely changes the  $\chi^2$  and AICC values (compared to those for models (i) and (iii), respectively). Thus, we cannot unambiguously determine whether the partial coverage effect is present or absent in the C I lines (at a  $1 \pm 1\%$  level) for this system.

## 7. COMPARISON OF OUR RESULTS WITH THE RESULTS OF PREVIOUS ANALYSES OF THIS SYSTEM

### 7.1. The $H_2$ Column Density in the Component A

The results of our analysis of the  $H_2$  system in the VLT spectrum of J 2123–0050 are compared with the results of the analyses of the  $H_2$  system in the Keck spectrum of J 2123–0050 [22, 23] in Table 1. The results differ mainly in  $H_2$  column density estimate for component A at the  $J = 0$  level.  $N_{H_2}^A(J=0)$  obtained in this paper is  $\log N_{H_2}^A(J=0) = 17.37 \pm 0.02$ , which exceeds the estimate from [23] by a factor of 3 ( $16.86 \pm 0.24$ ) and the estimate from [22] by a factor of 30 ( $15.80 \pm 0.40$ ). Different quality of the spectra and different allowance for the Ly $\alpha$ -forest absorption lines overlapping with the  $H_2$  lines can be responsible for the difference between the results of our analysis and those of [22, 23]. Among all the  $H_2$  lines of the transitions from the  $J = 0$  level accessible to analysis, only two lines, L0R0 and L3R0, do not overlap with the Ly $\alpha$ -forest lines. Figure 9 shows the profiles for the  $H_2$  absorption lines of the transitions from the  $J = 0$  level for the Keck (upper panel) and VLT (lower panel) spectra. The solid curve indicates the synthetic spectrum of the  $H_2$  system constructed using the  $H_2$  column densities determined in this paper. The Ly $\alpha$ -forest lines in the profiles for the  $H_2$  lines of the L2R0 and L4R0 transitions are seen to fall into the  $H_2$  line wing, while the Ly $\alpha$ -forest lines for the L1R0 and L6R0 transitions are located near the  $H_2$  line center. To determine the  $H_2$  column density at the  $J = 0$  level by comparing the observed spectrum with the synthetic one using all of the accessible  $H_2$  lines, it is necessary to artificially add the Ly $\alpha$ -forest absorption lines to the synthetic spectrum of the  $H_2$  system. The spectral parameters ( $N$  and  $b$ ) and the number of components for the unsaturated Ly $\alpha$ -forest lines cannot be unambiguously determined in most cases, because such systems belong to the root part of the curve of growth. Therefore, disregarding or, conversely, overusing the Ly $\alpha$ -forest lines in the analysis can lead to an overestimation or underestimation of the  $H_2$  column density being determined, respectively.

### 7.2. The $HD/2H_2$ ratio

Using the total  $H_2$  and HD column densities in component A,  $\log N_{H_2}^A = 17.94 \pm 0.01$  and  $\log N_{HD}^A = 13.87 \pm 0.06$ , we determined the  $HD/2H_2$  ratio for component A,

$N_{HD}^A/2N_{H_2}^A = (4.26 \pm 0.60) \times 10^{-5}$ . This value is lower than that measured by [23],  $(7.9 \pm 4.6) \times 10^{-5}$ , but it exceeds the primordial deuterium abundance estimated by [45],  $(2.62 \pm 0.15) \times 10^{-5}$ , by almost 3 standard deviations. Figure 10 compares the measured  $N_{HD}/2N_{H_2}$  in the absorption systems in the spectra of quasars at  $z_{abs} > 2$  and in the systems of our Galaxy. The data were taken from Table 2 in [9] (quasars) as well as [11, 46] (our Galaxy). At present, the  $H_2/HD$  system being investigated is the only one in which the  $N_{HD}/2N_{H_2}$  ratio exceeds the primordial deuterium abundance estimate. The possible explanations of such a high value are most likely related to the chemistry of molecular clouds; more specifically, under certain physical conditions in the cloud, the deuterium molecular fraction can exceed the hydrogen molecular fraction ([47] see also Sect. 9.1).

## 8. PHYSICAL CONDITIONS IN THE MOLECULAR CLOUDS J 2123–0050 A AND B

### 8.1. The UV Background Intensity

The upper rotational levels of  $H_2$  molecules with  $J = 3, 4$ , and  $5$  are populated mainly through radiative pumping (see, e.g., [48]). The  $H_2$  rotational level population diagrams for components A and B are shown in Fig. 5. Component A with a high column density corresponds to the optically thick case [49], while component B has a low column density and represents the optically thin case [50]. In the optically thin case, the shielding of UV radiation is negligible. This allows a simple estimate of the UV background intensity to be obtained within the framework of a homogeneous model, where the gas number density and the UV background intensity are assumed to be constant over the cloud volume. In the optically thick case, as the depth of radiation penetration into the cloud increases, the UV background intensity can decrease by several orders of magnitude due to the effect of shielding by  $H_2$  molecules (see, e.g., [51, 52]). At the center of an optically thick cloud, the  $H_2$  molecules are predominantly at the lower  $J = 0$  and  $1$  rotational levels, while the  $H_2$  molecules near the cloud boundary can strongly populate the upper  $J = 3, 4$ , and  $5$  rotational levels (see, e.g., [51, 32]). Therefore, numerical simulations, for example, with the Meudon PDR [52] or CLOUDY [53] codes, should be used for detailed calculations. Our calculation within the homogeneous model gives only an approximate estimate.

The component B represents the optically thin case that can be described in the approximation of a homogeneous cloud. The ortho- ( $J = 1, 3, 5$ ) and para- ( $J = 2, 4, 6$ ) hydrogen level populations are determined by radiative pumping,  $H_2$  collisions with H atoms, and spontaneous transitions:

$$N_{H_2}^{J=0} \beta p_{4,0} + N_{H_2}^{J=2} (n_H k_{24} + \beta p_{4,2}) = N_{H_2}^{J=4} (A_{42} + n_H k_{42} + \beta (p_{2,4} + p_{0,4})) \quad (3)$$

$$N_{H_2}^{J=1} \beta p_{5,0} + N_{H_2}^{J=3} (n_H k_{35} + \beta p_{5,3}) = N_{H_2}^{J=5} (A_{53} + n_H k_{53} + \beta (p_{3,5} + p_{1,5})) \quad (4)$$

where  $\beta$  is the photoabsorption rate,  $k_{24}$  and  $k_{42}$  are the collisional rate coefficients for the transitions between

the  $\text{H}_2$  levels ( $2 \rightarrow 4$ ) and ( $4 \rightarrow 2$ ),  $k_{35}$  and  $k_{53}$  are those for the transitions between the  $\text{H}_2$  levels ( $3 \rightarrow 5$ ) and ( $5 \rightarrow 3$ ),  $p_{4,0} = 0.26$ ,  $p_{2,4} = 0.32$ ,  $p_{4,2} = 0.32$ ,  $p_{0,4} = 0.08$ ,  $p_{5,1} = 0.12$  and  $p_{5,3} = 0.21$  are the radiative pumping rate coefficients [50], and  $A_{42} = 2.79 \times 10^{-9} \text{ s}^{-1}$  and  $A_{53} = 9.8 \times 10^{-9} \text{ s}^{-1}$  are the spontaneous transition probabilities [54]. For a temperature of  $\sim 200 \text{ K}$ ,  $k_{24} = 8.8 \times 10^{-16}$  and  $k_{42} = 1.8 \times 10^{-13}$ ,  $k_{35} = 6 \times 10^{-17}$  and  $k_{53} = 5 \times 10^{-14}$  in units of  $\text{cm}^3 \text{ s}^{-1}$  [55]; therefore, for a gas number density  $n_{\text{H}} < 100 \text{ cm}^{-3}$ , the contribution to the populations of the  $J = 4$  and  $5$  level through the collisions of  $\text{H}$  and  $\text{H}_2$  is negligible. The photoabsorption rate of UV radiation in the cloud can then be estimated as

$$\beta_{J=4} = \frac{N_{\text{H}_2}^{J=4} A_{42}}{N_{\text{H}_2}^{J=0} p_{4,0} + N_{\text{H}_2}^{J=2} p_{4,2}}, \quad (5)$$

$$\beta_{J=5} = \frac{N_{\text{H}_2}^{J=5} A_{53}}{N_{\text{H}_2}^{J=1} p_{5,1} + N_{\text{H}_2}^{J=3} p_{5,3}}. \quad (6)$$

Using  $N_{\text{H}_2}^J$  from Table 2, we obtain  $\beta = 1.8 \times 10^{-9} \text{ s}^{-1}$  (for  $J=4$ ) and  $\beta = 2.1 \times 10^{-9} \text{ s}^{-1}$  (for  $J=5$ ).

The photoabsorption rate  $\beta$  is related to the intensity of external UV radiation by the following relation:  $\beta = 4\pi \times 10^9 J_{\text{UV}} S_{\text{shield}}(N_{\text{H}_2})$ , where  $J_{\text{UV}}$  ( $\text{erg s}^{-1} \text{ cm}^2 \text{ Hz}^{-1} \text{ rad}^{-1}$ ) is the intensity of UV radiation with energy  $E = 12.87 \text{ eV}$  averaged over the solid angle [56], and  $S_{\text{shield}}(N_{\text{H}_2})$  is the factor that takes into account the self-shielding of the  $\text{H}_2$  cloud from the UV background [57]<sup>8</sup>. The mean UV background intensity in our Galaxy is  $J_{\text{UV}}^{\text{G}} \simeq 3.2 \times 10^{-20} \text{ erg s}^{-1} \text{ cm}^2 \text{ Hz}^{-1} \text{ rad}^{-1}$  (see, e.g., [44, 58]). Using the  $\text{H}_2$  column density at the cloud center,  $\log N_{\text{H}_2}^{\text{B}} = 14.86$ , we find that the intensity of the external UV background in component B is higher than the mean Galactic value by a factor of  $\chi_{\text{UV}} = J_{\text{UV}}/J_{\text{UV}}^{\text{G}} = 8.3$ .

### 8.2. The Gas Number Density for Components A and B

Using the  $\text{C I}$  fine-structure level populations, we can estimate the gas number density and temperature in the cloud and the UV background intensity. In calculating the balance of  $\text{C I}$  level populations, we took into account the interaction of  $\text{C I}$  atoms with cosmic microwave background radiation (CMBR) photons ( $T_{\text{CMB}} = 2.725 \times (1+z) = 8.34 \text{ K}$ ), the radiative pumping by UV radiation, and the collisions of  $\text{C I}$  atoms with  $\text{H I}$ ,  $\text{H}_2$ , and  $\text{He}$  [59]. The collision rate coefficients were taken from [60] (for  $\text{H}$ ), [61] (for ortho- and para-hydrogen), and [62] (for  $\text{He}$ ). The radiative pumping rate coefficients  $\Gamma_{01}$  and  $\Gamma_{02}$  [59] were multiplied by the factor  $\chi_{\text{UV}}$ . Since the  $\text{C I}$  column density is low ( $\log N \sim 14$ ), the  $\text{C I}$  self-shielding effect may be neglected.

For constant values of the gas molecular fraction and the helium abundance, the relative level populations  $n_{\text{C I}^*}/n_{\text{C I}}$  and  $n_{\text{C I}^{**}}/n_{\text{C I}}$  depend only on the gas number density, temperature, and  $\chi_{\text{UV}}$ . The upper panels in

Fig. 11 show the confidence regions for the number density and the UV background intensity (the gas temperature was assumed to be equal to the values corresponding to the ortho-to-para-hydrogen ratio,  $T_{01}^{\text{A}} = 139 \text{ K}$  and  $T_{01}^{\text{B}} = 648 \text{ K}$ , see Section 4.1). The lower panels in Fig. 11 show the confidence regions for the number density and temperature (the UV background was assumed to be  $\chi_{8.3}$ , which corresponds to the background estimate in component B; see the previous section). The helium abundance for both components was assumed to be  $n_{\text{He}}/n_{\text{H}} = 0.083$  (the primordial abundance; see, e.g., [63]), while the gas molecular fraction was  $f_{\text{H}_2}^{\text{A}} = 0.1$  for component A (the mean value for the sub-DLA system) and  $f_{\text{H}_2}^{\text{B}} = 0.001$  for component B.

As shown on the upper panel in Fig. 11, the gas number density for component A depends weakly on the UV background if  $\chi_{\text{UV}} \leq 10$ . The best value is  $n_{\text{A}} = 30 \pm 10 \text{ cm}^{-3}$ . If the UV background in component A is close to the value determined for component B (see the lower panel in Fig. 11), then we cannot unambiguously determine the physical conditions: the gas can be hot and rarefied ( $T \sim 500 \text{ K}$  and  $n \sim 10 \text{ cm}^{-3}$ ) or cold and denser ( $T \sim 50 \text{ K}$  and  $n \sim 50 \text{ cm}^{-3}$ ). The accuracy of determining  $n$  and  $T$  corresponds to a change in the  $N_{\text{C I}^*}/N_{\text{C I}}$  and  $N_{\text{C I}^{**}}/N_{\text{C I}}$  ratios within one standard deviation.

For component B, if we assume  $T = T_{01}^{\text{B}} \sim 650 \text{ K}$  and  $\chi_{\text{UV}} \sim 8.3$ , the gas number density is determined with a high accuracy,  $n_{\text{B}} \sim 26 \pm 4 \text{ cm}^{-3}$  (see the upper right panel in Fig. 11). However, the ortho-para-hydrogen ratio in the optically thin case is known to be insensitive to the kinetic temperature of the gas (see, e.g., [51]); therefore, the gas temperature in the cloud can differ from  $T_{01}^{\text{B}}$ . If the gas temperature is limited,  $T \geq 100 \text{ K}$ , then our analysis of the  $\text{C I}$  level populations gives an estimate of the gas number density  $n \leq 100 \text{ cm}^{-3}$ .

### 8.3. The $\text{H}_2$ Formation Rate on Dust in Component A

Under the condition of a stationary balance in the cloud, the numbers of  $\text{H}_2$  molecules formed on dust and destroyed by UV radiation are

$$R_{\text{H}_2} n_{\text{H}} n = 0.11 \beta n_{\text{H}_2}, \quad (7)$$

where  $R_{\text{H}_2}$  is the  $\text{H}_2$  formation rate coefficient on dust,  $n = n_{\text{H}} + 2n_{\text{H}_2}$  is the total hydrogen number density, and  $\beta$  is the photoabsorption rate. The photoabsorption rate in the cloud  $\beta$  is related to the intensity of the external UV background by the following relation:  $\beta = 4 \times 10^{-10} \times \chi_{\text{UV}} \times S_{\text{shield}}(N_{\text{H}_2}) \text{ s}^{-1}$ . Usually, the hydrogen molecular fraction in interstellar clouds increases toward the center; therefore, the column density ratio  $N_{\text{H}_2}^{\text{A}}/N_{\text{H I}} = 0.05$  can be used as a lower limit on  $n_{\text{H}_2}/n_{\text{H}}$  at the cloud center. For the central part of the cloud ( $\log N_{\text{H}_2} = 17.6$ ,  $S_{\text{shield}} = 1.2 \times 10^{-3}$ ), we then obtain

$$\frac{R_{\text{H}_2} n}{\chi_{\text{UV}}} = 2.6 \times 10^{-15} \times \frac{n_{\text{H}_2}/n}{(0.05)} \text{ s}^{-1} \quad (8)$$

It follows from our analysis of the  $\text{C I}$  level populations that if the UV background in component A does not exceed  $\chi_{\text{UV}} \approx 10$ , then the gas number density is  $n_{\text{A}} = 30 \pm 10 \text{ cm}^{-3}$ . We then obtain an estimate of

<sup>8</sup> For  $\log N_{\text{H}_2} > 14$ :  $S_{\text{shield}}(N_{\text{H}_2}) = 0.965/(1+x/b_5)^2 + 0.035/(1+x)^{0.5} \times \exp(-8.5 \times 10^{-4}(1+x)^{0.5})$ , where  $x = N/5 \times 10^{14} \text{ cm}^{-2}$ ,  $b_5 = b/10^5 \text{ cm s}^{-1}$



$R_{\text{H}_2} \times \chi_{\text{UV}}^{-1} = 8.8 \times 10^{-17} \text{ cm}^3 \text{ s}^{-1}$ . For comparison, the mean  $\text{H}_2$  formation rate measured in molecular clouds in our Galaxy is  $R_{\text{H}_2}^{\text{G}} = (3 - 4) \times 10^{-17} \text{ cm}^3 \text{ s}^{-1}$  [50, 64]. Thus, for the observed amount of  $\text{H}_2$  to be formed in the sub-DLA system being investigated at the mean Galactic value of  $R_{\text{H}_2}$ , the UV background intensity must be a factor of 2.3 lower than the mean Galactic one. However, it follows from our simulations of component A with the Meudon PDR code (see below) that the UV background intensity must be a factor of  $\sim 12$  higher than the mean Galactic value. Using this value, we obtained an estimate of the  $\text{H}_2$  formation rate coefficient on dust in component A,  $R_{\text{H}_2}^{\text{A}} = 1.1 \times 10^{-15} \text{ cm}^3 \text{ s}^{-1}$ , which is a factor of  $\sim 35$  higher than the mean Galactic value.

#### 8.4. The Gas Ionization Fraction

For low  $\text{H}_2$  column densities ( $\log N_{\text{H}_2} \leq 20$ ), absorption in the  $\text{H}_2$  lines of the Lyman and Werner bands changes insignificantly the number of UV photons capable of destroying HD and ionizing C I (see, e.g., [65]). Therefore, the HD and C I abundances in the medium correspond to their equilibrium values, which depend on the e. and  $\text{H}^+$  number densities, i.e., the gas ionization fraction.

HD molecules are formed in the reaction of collisions between  $\text{H}_2$  and  $\text{D}^+$ , while the abundance of  $\text{D}^+$  ions in a gas with a low molecular fraction is established according to the chemical equilibrium of the direct and reverse reactions  $\text{H}^+ + \text{D} \rightleftharpoons \text{H} + \text{D}^+$  (see, e.g., [43]). Assuming that the cloud is homogeneous and that the HD and  $\text{H}_2$  molecules belong to the same spatial region, i.e.,  $N_{\text{HD}}/N_{\text{H}_2} \approx n_{\text{HD}}/n_{\text{H}_2}$ , we can calculate the number density of  $\text{H}^+$  ions from the following formula (see, e.g., [43]):

$$n_{\text{H}^+} = \frac{\beta(\text{HD})N_{\text{HD}}}{k_{\text{H}_2+\text{D}^+}N_{\text{H}_2}(\text{D}/\text{H})\frac{k_1}{k_2}}, \quad (9)$$

where  $\beta(\text{HD}) = \chi_{\text{UV}} \times 1.5 \times 10^{-11} \text{ s}^{-1}$  is the HD photodestruction rate ( $\chi_{\text{UV}}$  is measured with respect to the intensity of the mean Galactic UV background from [44]),  $k_{\text{H}_2+\text{D}^+} = 2 \times 10^{-9} \text{ cm}^3 \text{ s}^{-1}$  is the HD formation rate,  $\text{D}/\text{H} = 3 \times 10^{-5}$  is the atomic deuterium abundance for systems at high  $z$ , and  $k_1/k_2 = \exp(-41/T)$  is the ratio of the direct and inverse  $\text{H}^+$  and D collision reaction rates. Using the gas temperature estimated from the ortho-to-para hydrogen ratio,  $T_{01} = 140 \text{ K}$ , and the UV background intensity estimated from our simulations of component A with the Meudon PDR code,  $\chi_{\text{UV}} = 12$  (see Sect. 9.1), we obtain  $n_{\text{H}^+} \simeq 0.3 \text{ cm}^{-3}$ .

Neutral carbon is formed in the recombination reaction of  $\text{C}^+$  ions with electrons and/or polyaromatic hydrocarbons (PAHs) (see, e.g., [66]). However, the contribution from the recombination reaction of  $\text{C}^+$  with PAHs has not been completely established to date (for a discussion and references, see [67]). If this reaction channel is disregarded, then the electron number density in the gas is expressed in terms of the C I photodestruction rate  $\beta(\text{C}) = \chi_{\text{UV}} \times 2.1 \times 10^{-10} \text{ s}^{-1}$ , the  $\text{C}^+$  recombination coefficient  $\alpha(\text{C}^+) = 1.8 \times 10^{-11} (T/100)^{-0.83} \text{ cm}^3 \text{ s}^{-1}$  (for  $20 \text{ K} < T < 140 \text{ K}$ ; see [66]), and the ratio of the C I and  $\text{C}^+$  number densities:

$$n_{\text{e}^-} = \frac{\beta(\text{C})N_{\text{C I}}}{\alpha(\text{C}^+)N_{\text{C}^+}}, \quad (10)$$

For  $\chi_{\text{UV}} = 12$  and  $T = 140 \text{ K}$ ,  $\log N_{\text{C I}} = 14.06$ , and  $\log N_{\text{C}^+} = 16.25$ , we obtain  $n_{\text{e}^-} \simeq 1.2 \text{ cm}^{-3}$ . Assuming that the gas molecular fraction for component A is  $f_{\text{H}_2}^{\text{A}} = 0.1$  and the number density is  $n^{\text{A}} = 30 \text{ cm}^{-3}$ , we obtain  $n_{\text{e}^-}/n_{\text{H}} \sim 4 \times 10^{-2}$ . Thus, in comparison with the values measured in diffuse clouds in our Galaxy with a similar gas number density ( $n_{\text{e}^-}/n_{\text{H}} \leq 6.6 \times 10^{-3}$ , see [41] and  $n_{\text{e}^-}/n_{\text{H}} \leq 10^{-6}$ ), the gas ionization fraction in component A turns out to be higher by almost an order of magnitude.

## 9. SIMULATIONS OF THE MOLECULAR CLOUD STRUCTURE

The estimates of the physical conditions obtained within the homogeneous model (Section 8) are often approximate. For more proper estimates, we performed simulations of the molecular cloud structure with the Meudon PDR and CLOUDY codes.

### 9.1. Simulations of the Molecular Clouds with the Meudon PDR Code

By comparing the observed H I,  $\text{H}_2$ , HD, and C I column densities and the  $\text{H}_2$  and C I level population diagrams with the results of our Meudon PDR simulations, we determined the physical conditions in the components of the  $\text{H}_2$  absorption system. In comparison with the homogeneous model, where the physical conditions and the concentrations of species are assumed to be constant over the cloud volume, the code takes into account the shielding of UV radiation in absorption lines and the shielding on dust and consistently solves the thermal, ionization, and chemical balance equations in the medium (by an iterative method). The cloud is represented as plane-parallel layers of gas and dust with a constant proton density in each layer ( $n_{\text{p}} = n_{\text{H}} + 2n_{\text{H}_2} + n_{\text{H}^+}$ ).

For the spectrum of the background UV radiation, we used the model proposed by [68]. The radiation spectrum spans the wavelength range  $912 - 8000 \text{ \AA}$ . The radiation with a wavelength below  $912 \text{ \AA}$  in the photodissociation region is believed to be shielded by a layer of atomic hydrogen and, therefore, is disregarded. The UV background intensity with respect to the mean Galactic value  $J_{\text{UV}}^{\text{G}} \simeq 3.2 \times 10^{-20} \text{ erg s}^{-1} \text{ cm}^2 \text{ Hz}^{-1} \text{ rad}^{-1}$  taken from [44] was specified by the parameter  $\chi_{\text{UV}}$ . In addition to the UV radiation, the cloud is irradiated by the CMBR and the cosmic-ray (CR) background. The CMBR temperature was assumed to be  $2.725 \times (1 + z_{\text{abs}}) = 8.34 \text{ K}$ . The CR background intensity with respect to the mean Galactic value  $2 \times 10^{-16} \text{ s}^{-1}$  (see, e.g., [69]) was specified by the parameter  $\xi_{\text{CR}}$ . It is important to note that in the Meudon PDR code the gas is ionized by CRs. Therefore, CR is the key parameter defining the ionization fraction and, consequently, the number of HD molecules and C I atoms in the cloud being investigated (see Section 8.4).

In our simulations, we used the abundances of elements in the cloud (He, C, N, S, Si, Fe, etc.) corresponding to the mean gas metallicity in the sub-DLA system ( $[\text{X}/\text{H}] = -0.2$ ; see [5]). Among these elements, carbon plays a special role in calculating the thermal balance, because the emission from  $\text{C}^+$  ions in the  $\lambda = 158 \mu\text{m}$

line is a major gas cooling process in the interstellar medium [70]. However, since the C II absorption line is strongly saturated, we cannot determine what part of the total C<sup>+</sup> column density belongs to the molecular clouds being investigated. Therefore, we varied the carbon abundance in the cloud in a range of values corresponding a total carbon column density in the cloud from  $\log N_{\text{C}}^{\text{tot}} = 14.5$  ( $10^{-2}$  of the solar abundance) to  $\log N_{\text{C}}^{\text{tot}} = 16.25$  (the upper limit for  $\log N_{\text{C}}^{\text{tot}}$  in the sub-DLA system). At the same time, the abundances of other elements were not varied. The carbon abundance with respect to the solar one,  $(\text{C}/\text{H})_{\odot} = 2.7 \times 10^{-4}$  [71], was specified by the parameter  $X_{\text{C}}$ . The deuterium abundance was assumed to be  $(\text{D}/\text{H}) = 3 \times 10^{-5}$ , which corresponds to the typical D abundance at high redshifts in molecular clouds (see, e.g., [9]).

Dust is one of the most important components in the interstellar medium; its properties affect the heating rate of the medium (through the photo-electric reaction on dust), the gas shielding from UV radiation, and the H<sub>2</sub> formation rate. The model from [72] was used for the grain size distribution. The absorption of UV radiation on dust was described using an extinction model for the SMC,  $R_{\text{V}} = 2.87$  (this model is believed to describe well the reddening of quasar spectra; see, e.g., [73]). The amount of dust on the line of sight was determined via the interstellar extinction parameter  $A_{\text{V}} = R_{\text{V}}E(B - V)$ , which was set equal to 0.115 mag, corresponding to a certain upper limit on the spectrum reddening (color excess),  $E(B - V) = 0.04$  [65]. The dust number density in the cloud governing the gas heating and the H<sub>2</sub> formation rate is determined using the dust-to-gas ratio  $G$ . We used three values:  $G = 0.01, 0.02$ , and  $0.1$ , corresponding to 1, 2, and 10 mean Galactic values [74]. The H<sub>2</sub> formation in the Meudon PDR code is computed using two mechanisms: Langmuir-Hinshelwood and Eley-Rideal (see [75]). However, as is pointed out in [75], the detailed description of H<sub>2</sub> formation is still missing. Therefore, we used two approaches: (i) a “numerical calculation” according to the Langmuir-Hinshelwood and Eley-Rideal models and (ii) an “approximate calculation” where the H<sub>2</sub> formation rate was specified by some value constant over the cloud volume:  $R_{\text{H}_2} = R_0 \times 3 \times 10^{-17} \text{ cm}^3 \text{ s}^{-1}$  (with respect to the mean Galactic value; see [50]). The latter approach allows the possibility of a difference between the properties of dust in a high-redshift cloud and in our Galaxy to be taken into account qualitatively without going into the specific properties of dust grains (the size distribution, the reflection coefficient, the sticking coefficient, the density, etc.).

### 9.1.1. Simulations of the cloud J2123–0050 A

The DLA systems have much larger sizes than the molecular clouds: the sizes of the DLA systems are estimated to be several 10 kpc [3], while the sizes of the H<sub>2</sub> clouds are  $\sim 1$  pc (see, e.g., [26]). Therefore, the DLA system occupies a larger region than does the H<sub>2</sub> system on the line of sight (with the H<sub>2</sub> cloud being located inside the DLA system). Consequently, we cannot reliably determine what fraction of the entire HI column density belongs to the H<sub>2</sub> cloud by measuring the total HI and H<sub>2</sub> column densities. Since the sub-DLA system being

investigated has the lowest HI column density (almost two orders of magnitude lower than the mean  $N_{\text{HI}}$ ; see Fig. 1) among the sub-DLA and DLA systems containing H<sub>2</sub> and, at the same time, the H<sub>2</sub> column density in component A is fairly high (close to the mean  $N_{\text{H}_2}$ ), in our simulations we assume that the entire observed HI in the sub-DLA system belongs to the H<sub>2</sub> cloud. Therefore, the total hydrogen column density ( $N_{\text{HI}} + 2N_{\text{H}_2}$ ) was taken to be  $\log N = 19.22$ .

We used two thermodynamic cloud models: (I) with a constant pressure and (II) with a constant hydrogen density. The pressure was assumed to be  $(8.4 \times 10^3) \text{ cm}^{-3} \text{ K}$ , which corresponds to the upper limit determined by analyzing the C I level populations. The hydrogen number density was assumed to be  $40 \text{ cm}^{-3}$ , which roughly corresponds to the conditions in the cloud. The second model describes the situation where H<sub>2</sub> is formed in the compression region, which was formed, for example, through the gas interaction with the shock front.

For each model, we performed our calculations for a grid of parameters  $\chi_{\text{UV}}$ ,  $\zeta_{\text{CR}}$ ,  $R_0$ ,  $X_{\text{C}}$  and  $G$ . The model with a constant density gives the best description for the following set of parameters:  $\chi_{\text{UV}} = 12$ ,  $\zeta_{\text{CR}} = 5 \times 10^2$ ,  $R_0 = 38$ ,  $X_{\text{C}} = 2.8$  and  $G = 0.01$  (model (f) in Table 5). The model simultaneously reproduces the observed column densities of the species and the H<sub>2</sub> and C I level populations. Table 5 and Fig. 12 compare the results of our simulations for the six most characteristic cases: (a–e) correspond to the isobaric models, (f) corresponds to the model with a constant density.

#### Main inconsistencies of the isobaric models.

Using an isobaric model, we can obtain H<sub>2</sub>, HD, and C I column densities close to the observed ones (models (ñ) and (e)), but we fail to satisfactorily describe the H<sub>2</sub> and C I level population diagrams.

Models (a) and (b) correspond to the case where the medium is irradiated by an UV background with a low intensity,  $\chi_{\text{UV}} = 0.4$  and  $1.2$ . In these models, the populations of H<sub>2</sub> levels with  $J \geq 3$  are more than an order of magnitude lower than the observed values, despite the fact that the total H<sub>2</sub> column density is close to or even higher than the measured value. An additional level population can be provided through radiative pumping with a higher UV background intensity<sup>9</sup>. Note that the column density of HD molecules can be described in these models, but the C I column density turns out to be lower by more than two orders of magnitude.

Model (ñ) describes a cloud irradiated by an UV background with an intensity higher than the mean Galactic one by a factor of 5. A high UV background increases the gas heating, which in this model is compensated for by an enhanced carbon abundance ( $X_{\text{C}} = 1.9$ ), because carbon is the main coolant of the medium. The model yields H<sub>2</sub> and C I column densities close to the observed ones. However, the derived HD column density and the H<sub>2</sub> and C I level populations are inconsis-

<sup>9</sup> Apart from the population mechanism for high H<sub>2</sub> levels through radiative pumping, other mechanisms that are disregarded in the Meudon PDR code are considered in the literature. For example, the excitation of H<sub>2</sub> molecules when the gas is compressed and heated due to the interaction of the molecular cloud with turbulence and/or a C-shock (see [76, 77, 78]).

**Table 5.** Results of our simulations of the absorption system J 2123-0050 A.  $\chi_{\text{UV}}$ ,  $\zeta_{\text{CR}}$  and  $R_0$  – are the UV background intensity, the CR background intensity, and the  $\text{H}_2$  formation rate with respect to their mean Galactic values;  $X_{\text{C}}$  is the carbon abundance with respect to the solar one;  $n$  and  $T$  are the number density and temperature at the cloud center. \* – The range of the formation rate coefficient  $R_0$  calculated numerically according to the model from [75] is specified.

No.	$\chi_{\text{UV}}$	$\zeta_{\text{CR}}$	$X_{\text{C}}$	$R_0$	$n, \text{cm}^{-3}$	$T, \text{K}$	$N_{\text{H}^+}/N_{\text{H}}$
a	0.4	1	0.02	1.7-3.0*	73	115	$4.7 \times 10^{-4}$
b	1.2	1	0.2	1.7-2.2*	47	180	$6.0 \times 10^{-3}$
c	5	1	1.8	1.7-1.9*	165	51	$1.5 \times 10^{-4}$
d	12	5	3.7	0.5-0.9*	180	47	$1.7 \times 10^{-4}$
e	12	$5 \times 10^2$	3.0	10	124	68	$4.7 \times 10^{-3}$
f	12	$5 \times 10^2$	2.8	38	40	145	$1.1 \times 10^{-2}$

No.	$\log N_{\text{H}_2}$	$\log N_{\text{CI}}$	$\log N_{\text{HD}}$	$N_{\text{H}_2}^{\text{J}=1}/N_{\text{H}_2}^{\text{J}=0}$	$\log N_{\text{H}_2}^{\text{J}=4}$	$\log N_{\text{H}_2}^{\text{J}=5}$	$N_{\text{CI}^*}/N_{\text{CI}}$
a	18.8	11.4	14.2	2.0	13.0	12.5	0.4
b	18.0	11.7	13.5	3.1	13.0	12.6	0.4
c	17.7	13.7	12.8	0.4	13.7	13.1	0.7
d	14.6	14.0	10.6	1.1	13.1	12.9	0.7
e	17.8	14.3	13.9	0.7	14.1	13.7	0.7
f	17.9	14.0	14.0	2.6	14.1	13.8	0.4

**Table 6.** Results of our simulations of the absorption system J 2123-0050 B. The notation is the same as that in Table 5. \* – The range of the formation rate coefficient  $R_0$  calculated numerically according to the model from [75] is specified.

No.	$\chi_{\text{UV}}$	$\zeta_{\text{CR}}$	$R_0$	$X_{\text{C}}$	$\log N_{\text{H}}^{\text{tot}}$	$\log N_{\text{H}_2}$	$\log N_{\text{CI}}$	$\log N_{\text{H}_2}^{\text{J}=4}$	$\log N_{\text{H}_2}^{\text{J}=5}$
g	1.5	1	5.2-8.9*	0.02	19.2	15.7	9.8	12.7	12.3
h	12	1	43	2.8	18.7	15.2	12.0	13.6	13.4
i	12	$1.5 \times 10^2$	43	2.8	18.7	15.2	12.9	13.6	13.4

tent with the measured values. The populations of the  $\text{J} = 4$  and  $5$  levels turn out to be a factor of 3 higher than those in models (a) and (b), but still a factor of 2 – 3 lower than the observed values.

In model (d), the radiation intensity is even higher:  $\chi_{\text{UV}} \simeq 12$ . To compensate for the cloud heating, the carbon abundance was taken to be maximally high,  $X_{\text{C}} = 3.7$  (which corresponds to the case where the entire  $\text{C}^+$  column density in the sub-DLA system belongs to the molecular cloud). The gas number density and temperature be found the same as those in model (c). However, the obtained column density of  $\text{H}_2$  in model (d) is  $\log N_{\text{H}_2} \sim 15$ , that is less than the measured value by two orders of magnitude. First, the  $\text{H}_2$  column density is too low to shield the molecules from UV radiation; second, at the same  $\text{H}_2$  formation rate as that in model (c), the photodestruction rate turns out to be higher (see Eq. (7)).

In models (a)–(d), we used the “numerical calculation” according to the model from [75], with the dust-to-gas ratio in the medium  $G = 0.01$ , for the  $\text{H}_2$  formation. As  $G$  increases, the  $\text{H}_2$  formation rate coefficient and the efficiency of gas heating by UV radiation increase proportionally. Despite the fact that the  $\text{H}_2$  formation rate becomes higher, the gas number density decreases (due to the pressure constancy condition). Therefore, according to Eq. (7), increasing the dust content does not allow the problem of the formation of a large amount of molec-

ular hydrogen in a medium with a high UV background to be solved. In our calculations using an isobaric model with a high UV background, a high carbon abundance (as in model (d)), and  $G = 0.02$  and  $0.1$ , the gas turns out to be hot,  $T > 1000 \text{ K}$ , and rarefied,  $n \leq 1 \text{ cm}^{-3}$ . Virtually no  $\text{H}_2$  molecules are formed in such a medium.

The “approximate calculation”, where the  $\text{H}_2$  formation rate coefficient is specified by a value constant over the cloud volume and does not depend on the physical conditions, can be used for the  $\text{H}_2$  formation. Model (e) corresponds to this case. At  $R_0 \simeq 10$ ,  $\chi_{\text{UV}} = 12$  and  $X_{\text{C}} = 3$  we can simultaneously reproduce the total  $\text{H}_2$  column density and the upper level populations (see Table 5). However, in this model we fail to reproduce the physical conditions in the cloud: the gas turns out to be denser ( $n \geq 100 \text{ cm}^{-3}$ ) and colder ( $T \leq 60 \text{ K}$ ). As a consequence, the ratio of the populations of the first two  $\text{H}_2$  and  $\text{CI}$  levels is consistent with the measured  $\text{H}_2$  number densities, while the ratio of the  $\text{CI}^*$  and  $\text{CI}$  level populations is twice that measured in the component A.

#### The abundance of HD molecules and the gas ionization fraction

For models (a)–(d), the  $\text{HD}/2\text{H}_2$  ratio does not exceed  $10^{-5}$ , which is less than the observed value by almost an order of magnitude. Since HD is formed through the ion-molecular reaction ( $\text{H}_2 + \text{D}^+$ ), the HD formation rate increases with  $\text{H}^+$  number density, which in

the PDR models is determined mainly by the CR background intensity. The HD/2H<sub>2</sub> ratio is consistent with the measured value at a relative H<sup>+</sup> number density  $n_{\text{H}^+}/n_{\text{H}} \approx 10^{-2}$ , which corresponds to  $\zeta_{\text{CR}} = 5 \times 10^2$ , i.e., a factor of 500 more intense CR flux is needed. For  $\zeta_{\text{CR}} = 1$ , the gas ionization fraction in the Meudon PDR models is low,  $n_{\text{H}^+}/n_{\text{H}} \approx 10^{-4}$ , which is not enough for the HD formation in a medium with a high UV background intensity. A high  $\zeta_{\text{CR}}$  is probably not an estimate of the CR background intensity in the cloud, but only points to a high gas ionization fraction. Possible causes are discussed below in Section 9.2.

### The model with a constant density

In the model with a constant density (model (f)), we can simultaneously describe the H<sub>2</sub>, HD, and C I column densities and the H<sub>2</sub> and C I level populations. In this case, just as for the isobaric model, high UV and CR background intensities and a high carbon abundance are needed.

A detailed analysis of model (f) is presented in Fig. 13. The left panel shows the number densities of the species as a function of the distance from the cloud boundary. The H, H<sup>+</sup>, C<sup>+</sup>, and C I number densities barely change along the line of sight (due to the density constancy and the low gas molecular fraction). The right panels show the D and H molecular fractions (the upper panel: the local values are indicated by the solid lines, while the values averaged along the line of sight are indicated by the dashed lines) and the HD/2H<sub>2</sub> and D/H ratios (the lower panel). The HD formation rate in the cloud is higher than the H<sub>2</sub> formation rate due to the relatively high gas ionization fraction,  $\sim 10^{-2}$ . As a result, the local D and H molecular fractions at the cloud center turn out to be twice their mean values, and, consequently, the HD/2H<sub>2</sub> ratio is higher than the D/H ratio. This leads to the D/H abundance determined from the ratio of the atomic D I and H I column densities being lower than the isotropic D/H ratio ( $2.75 \times 10^{-5}$  versus  $3.0 \times 10^{-5}$ ). The sign and magnitude of the effect depend on the mean gas molecular fraction along the line of sight and the H<sup>+</sup> number density. For  $f_{\text{PH}_2} = 0.1$ , the  $N_{\text{DI}}/N_{\text{HI}}$  ratio can change within 10% of the isotropic ratio. The effect should be taken into account if a molecular cloud with the same redshift falls on the line of sight passing through the H I/D I absorption system. Obviously, in this case, the  $(N_{\text{DI}} + N_{\text{HD}})/(N_{\text{HI}} + 2N_{\text{H}_2})$  ratio is a proper estimate of (D/H).

#### 9.1.2. Simulations of the cloud J 2123–0050 B

For component B (just as for component A), we cannot determine what part of the measure H I column density associated with the molecular cloud. Therefore,  $N_{\text{HI}}^{\text{B}}$  was an additional free parameter and was determined from the simulation results. The H I column density in the sub-DLA system,  $\log N_{\text{HI}} = 19.18 \pm 0.15$ , was chosen as an upper limit for  $N_{\text{HI}}^{\text{B}}$ . The results of our simulations are presented in Table 6. Model (g) corresponds to the calculations with a constant gas pressure ( $8.4 \times 10^3 \text{ cm}^{-3} \text{ K}$ ); models (h) and (i) correspond to those with a constant number density ( $40 \text{ cm}^{-3}$ ). Figure 14 shows the H<sub>2</sub> level population diagrams for these models. Just as in the case of simulating component A, a high UV background intensity ( $\chi_{\text{UV}} \sim 12$ ) is

needed to describe the populations of upper rotational H<sub>2</sub> levels. In model (g), the UV background is low and the H<sub>2</sub> levels are populated mainly through the collisional mechanism. The populations of the lower H<sub>2</sub> levels turn out to be a factor of 3–5 higher than the observed ones, while the populations of the upper  $J = 4$  and 5 levels are an order of magnitude lower. If the UV background is high (models (h) and (i)), then the H<sub>2</sub> level population diagram describes the diagram measured for component B.

At a high UV background and a low gas number density, a high H<sub>2</sub> formation rate coefficient on dust is needed for the H<sub>2</sub> formation. In model (g), the H<sub>2</sub> formation was calculated according to [75]; in models (h) and (i), the formation rate coefficient was equal to  $R_0$ . For  $R_0 = 43$ , the H<sub>2</sub> column density in models (h) and (i) turns out to be close to the observed one. The gas ionization fraction in component B can be estimated from the C I abundance (see, e.g., Section 8.4). The observed C I column density in model (i) is reconstructed at  $n_{\text{e}}/n_{\text{H}} = (0.9 - 1) \times 10^{-2}$ , which corresponds to  $\zeta_{\text{CR}} = 1.5 \times 10^2$ .

### 9.2. The Ionization Structure of the sub-DLA System. The CLOUDY Code

The high value of  $\zeta_{\text{CR}}$  ( $5 \times 10^2$  for component A and  $1.5 \times 10^2$  for component B) obtained in our simulations with the Meudon PDR code seems unlikely and probably points only to a high gas ionization that can actually be caused by other sources, for example, hard UV or X-ray radiation, which cannot be taken into account in the simulations with the Meudon PDR code. However, this can be done with the CLOUDY code, which can compute the ionization of the system by taking into account the hard UV radiation. We simulated the structure of the sub-DLA system and checked whether the external UV radiation (which is shielded incompletely in the system due to the low H I column density) could cause a high gas ionization fraction ( $\sim 10^{-2}$ ) at the system's center, where the molecular cloud could be located.

The computation was performed within the framework of an isobaric model with a plane-parallel geometry. The gas is irradiated only on one side of the system. The radiation spectrum consists of several components: (i) the extragalactic background (the HM96 model; see [79]), (ii) the average Galactic background (the “ISM” model) with an intensity that is a factor of 12 higher than  $J_{\text{UV}}^{\text{G}} \simeq 3.2 \times 10^{-20} \text{ erg s}^{-1} \text{ cm}^2 \text{ Hz}^{-1} \text{ rad}^{-1}$  [44], and (iii) the CMBR at  $z = 2$ . The CR background intensity was equal to the mean Galactic value  $2 \times 10^{-16} \text{ n}^{-1}$  (see, e.g., [69, 80]). The abundances of heavy elements corresponded to the metallicity for the sub-DLA system,  $[\text{S}/\text{H}] = -0.2$ . Our simulations with the CLOUDY code also show the necessity of a high H<sub>2</sub> formation rate, which was assumed to be  $2.3 \times 10^{-15} \text{ cm}^3 \text{ s}^{-1}$ . Since the total hydrogen column density  $N_{\text{H}^+} + N_{\text{HI}} + 2N_{\text{H}_2}$  in the sub-DLA system cannot be determined (because H<sup>+</sup>, which accounts for as much as 90%, is undetectable), the computation was performed until the total neutral hydrogen column density  $N_{\text{HI}} + 2N_{\text{H}_2}$  reached  $10^{18.9}$  (half of  $N_{\text{HI}}^{\text{tot}}$  for the sub-DLA being investigated). The result of our simulations is shown in Fig. 15. The H<sup>+</sup>,

H I, and H<sub>2</sub> number density profiles are shown as a function of the distance from the system's center.

The total H<sup>+</sup> column density is  $\log N_{\text{H}^+} = 19.9$ , which is a factor of 10 higher than the H I column density, i.e., the neutral gas is formed only in a narrow region near the system's center, while the bulk of the system ( $\sim 90\%$ ) is ionized. The number density of H<sup>+</sup> ions decreases rapidly with distance from the boundary between the cold neutral and hot ionized phases (see Fig. 15) and changes from  $2.0 \text{ cm}^{-2}$  at the boundary to  $2 \times 10^{-2} \text{ cm}^{-2}$  at the system's center. The medium is ionized through its irradiation by the UV background; the CR contribution is negligible (the H<sup>+</sup>, H I and H<sub>2</sub> profiles barely change if the CR background is disregarded). Thus, despite the fact that the ion number density decreases rapidly with neutral cloud depth, the ionization fraction of the medium remains fairly high because of the small cloud size. The mean  $n_{\text{H}^+}/n_{\text{H}} \sim 10^{-2}$ , in agreement with the value derived in our Meudon PDR simulations for components A and B. Thus, partial shielding of the hard UV radiation by neutral hydrogen in the sub-DLA system can be responsible for the high gas ionization fraction found in our Meudon PDR simulations.

## 10. CONCLUSION

We performed an independent analysis of the H<sub>2</sub> absorption system at  $z_{\text{abs}} = 2.059$  in the VLT spectrum of the quasar J2123–0050. The H<sub>2</sub> system consists of two components ( $z_{\text{A}} = 2.05932(5)$  and  $z_{\text{B}} = 2.05955(2)$ ) with total column densities  $\log N_{\text{H}_2}^{\text{A}} = 17.94 \pm 0.01$  and  $\log N_{\text{H}_2}^{\text{B}} = 15.16 \pm 0.01$ . The lines of HD molecules are detected only in component A with a column density  $\log N_{\text{HD}}^{\text{A}} = 13.87 \pm 0.06$ . Our estimate of the H<sub>2</sub> column density in component A is twice the value, obtained by [23],  $\log N_{\text{H}_2}^{\text{A}} = 17.64 \pm 0.15$ . The results differ mainly by the estimate of the H<sub>2</sub> column density in component A at the J = 0 level. Using our estimate of  $\log N_{\text{H}_2}^{\text{A}}$ , we calculated the abundance of HD molecules:  $N_{\text{HD}}^{\text{A}}/2N_{\text{H}_2}^{\text{A}} = (4.26 \pm 0.60) \times 10^{-5}$ . This value is consistent, within the statistical error limits, with that measured by [23], but it exceeds the primordial deuterium abundance  $(\text{D}/\text{H})_{\text{Pr}} = (2.62 \pm 0.15) \times 10^{-5}$  estimated by [45] by almost three standard deviations, which may be due to the complex chemistry of the H<sub>2</sub> and HD molecules.

For component A, we detected the partial coverage effect for the H<sub>2</sub> lines located near the Ly $\beta$  and O VI emission lines. The residual flux is  $\sim 3\%$  of the total flux. Due to the low H<sub>2</sub> column density and low oscillator strength for transitions of L1-0 and L0-0 Lyman bands, allowance for the partial coverage effect affects weakly the H<sub>2</sub> column density being determined.

The C I lines associated with the H<sub>2</sub> system for the transitions from the ground and two excited states are detected in the VLT spectrum. Our analysis showed that the C I line structure consists of three components, each of which is associated with components A and B. The third additional component (with  $\log N_{\text{C I}}^{\text{C}} = 12.78 \pm 0.03$  and a large Doppler parameter  $b \sim 7 \text{ km/s}$ ) probably associated with the ionized part of the sub-DLA system and not with the H<sub>2</sub> system.

Using the observed H I, H<sub>2</sub>, HD, and C I column densities as well as the H<sub>2</sub> and C I level population diagrams for components A and B, we investigated the physical conditions in this system. The medium in component A is optically thick in H<sub>2</sub> lines and has a low number density ( $30 \pm 10 \text{ cm}^{-3}$ ) and temperature ( $T_{01} = 139 \pm 6 \text{ K}$ ). In such a medium, molecular hydrogen shields the UV radiation in lines in the cloud (the H<sub>2</sub> photodestruction rate inside and at the edge of the cloud can differ by several orders of magnitude); therefore, we used our simulations with the Meudon PDR code to properly determine the physical conditions with allowance made for the UV background transfer inside the cloud. Using the model with a constant gas density  $n = 40 \text{ cm}^{-3}$ , a high UV background ( $\chi_{\text{UV}} \sim 12$  in units of the mean Galactic value), a high gas ionization fraction ( $n_{\text{H}^+}/n_{\text{H}} \sim 10^{-2}$ ), and a high H<sub>2</sub> formation rate coefficient on dust ( $R_{\text{H}_2} = 1.2 \times 10^{-15} \text{ cm}^3 \text{ s}^{-1}$ ), we can describe the observed parameters.

The high value of  $N_{\text{HD}}/2N_{\text{H}_2}$  in component A is due to the high gas ionization fraction ( $\sim 10^{-2}$ ), which is probably a unique feature of this sub-DLA system. Our simulations with the CLOUDY code show that such an ionization fraction can be a consequence of incomplete shielding of the UV radiation (with  $E > 13.6 \text{ eV}$ ) by neutral hydrogen in the sub-DLA system. A high gas ionization fraction leads to a significant increase in the HD formation rate. Therefore, even at a low gas molecular fraction,  $f_{\text{H}_2} \sim 0.1 - 0.2$ , the deuterium molecular fraction turns out to be higher than the hydrogen molecular fraction, which leads to the relation  $N_{\text{HD}}/2N_{\text{H}_2} > (\text{D}/\text{H})$ .

The medium in component B is optically thin in H<sub>2</sub> lines. In this case, the H<sub>2</sub> photodestruction rate barely changes with the depth of radiation penetration into the cloud. Using the homogeneous model, we estimated the UV background intensity in the cloud to be  $\chi_{\text{UV}} = 8.3$ . Our simulations with the Meudon PDR code for this component showed that the same high H<sub>2</sub> formation rate coefficient on dust as that in component A ( $R_{\text{H}_2} = 1.3 \times 10^{-15} \text{ cm}^3 \text{ s}^{-1}$ ) and a high gas ionization fraction ( $\sim 10^{-2}$ ) are needed to produce the observed amount of H<sub>2</sub> and C I at a high UV background ( $\chi_{\text{UV}} = 12$ ).

## 11. ACKNOWLEDGMENTS

This study was supported by the Russian Science Foundation (project no. 14-12-00955).

## References

- [1] Prochaska, J.X., Wolfe, A.M.: On the (Non)Evolution of H I Gas in Galaxies Over Cosmic Time. *ApJ***696** (2009) 1543–1547
- [2] Noterdaeme, P., Petitjean, P., Carithers, W.C., Pâris, I., Font-Ribera, A., Bailey, S., Aubourg, E., Bizyaev, D., Ebelke, G., Finley, H., Ge, J., Malanushenko, E., Malanushenko, V., Miralda-Escudé, J., Myers, A.D., Oravetz, D., Pan, K., Pieri, M.M., Ross, N.P., Schneider, D.P., Simmons, A., York, D.G.: Column density distribution and cosmological mass density of neutral gas: Sloan Digital Sky Survey-III Data Release 9. *A&A***547** (2012) L1
- [3] Krogager, J.K., Fynbo, J.P.U., Møller, P., Ledoux, C., Noterdaeme, P., Christensen, L., Milvang-Jensen, B., Sparre, M.: On the sizes of  $z \sim 2$  damped Ly $\alpha$  absorbing galaxies. *MNRAS***424** (2012) L1–L5
- [4] Meiring, J.D., Lauroesch, J.T., Kulkarni, V.P., Péroux, C., Khare, P., York, D.G., Crots, A.P.S.: New abundance de-

- terminations in  $z \leq 1.5$  QSO absorbers: seven sub-DLAs and one DLA. *MNRAS***376** (2007) 557–572
- [5] Milutinovic, N., Ellison, S.L., Prochaska, J.X., Tumlinson, J.: Ionization corrections in a multiphase interstellar medium: lessons from a  $z_{abs} \sim 2$  sub-DLA. *MNRAS***408** (2010) 2071–2082
- [6] Levshakov, S.A., Varshalovich, D.A.: Molecular hydrogen in the  $Z = 2.811$  absorbing material toward the quasar PKS 0528–250. *MNRAS***212** (1985) 517–521
- [7] Varshalovich, D.A., Ivanchik, A.V., Petitjean, P., Srianand, R., Ledoux, C.: HD Molecular Lines in an Absorption System at Redshift  $z=2.3377$ . *Astronomy Letters* **27** (2001) 683–685
- [8] Srianand, R., Noterdaeme, P., Ledoux, C., Petitjean, P.: First detection of CO in a high-redshift damped Lyman- $\alpha$  system. *A&A***482** (2008) L39–L42
- [9] Ivanchik, A.V., Balashev, S.A., Varshalovich, D.A., Klimenko, V.V.:  $H_2$ /HD molecular clouds in the early universe. An independent means of estimating the baryon density of the universe. *Astronomy Reports* **59** (2015) 100–117
- [10] Jenkins, E.B., Tripp, T.M.: The Distribution of Thermal Pressures in the Interstellar Medium from a Survey of C I Fine-Structure Excitation. *ApJS***137** (2001) 297–340
- [11] Snow, T.P., Ross, T.L., Destree, J.D., Drosback, M.M., Jensen, A.G., Rachford, B.L., Sonnentrucker, P., Ferlet, R.: A New FUSE Survey of Interstellar HD. *ApJ***688** (2008) 1124–1136
- [12] Rachford, B.L., Snow, T.P., Destree, J.D., Ross, T.L., Ferlet, R., Friedman, S.D., Gry, C., Jenkins, E.B., Morton, D.C., Savage, B.D., Shull, J.M., Sonnentrucker, P., Tumlinson, J., Vidal-Madjar, A., Welty, D.E., York, D.G.: Molecular Hydrogen in the FUSE Translucent Lines of Sight: The Full Sample. *ArXiv e-prints* (2008)
- [13] Noterdaeme, P., Srianand, R., Rahmani, H., Petitjean, P., Pâris, I., Ledoux, C., Gupta, N., López, S.: VLT/UVES observations of extremely strong intervening damped Lyman- $\alpha$  systems. Molecular hydrogen and excited carbon, oxygen, and silicon at  $\log N(H\text{ I}) = 22.4$ . *A&A***577** (2015) A24
- [14] Kruhler, T., Ledoux, C., Fynbo, J.P.U., Vreeswijk, P.M., Schmid, S., Malesani, D., Christensen, L., De Cia, A., Hjorth, J., Jakobsson, P., Kann, D.A., Kaper, L., Vergani, S.D., Afonso, P.M.J., Covino, S., de Ugarte Postigo, A., D’Elia, V., Filgas, R., Goldoni, P., Greiner, J., Hartoog, O.E., Milvang-Jensen, B., Nardini, M., Piranomonte, S., Rossi, A., Sánchez-Ramírez, R., Schady, P., Schulze, S., Sudilovsky, V., Tanvir, N.R., Tagliaferri, G., Watson, D.J., Wiersema, K., Wijers, R.A.M.J., Xu, D.: Molecular hydrogen in the damped Lyman  $\alpha$  system towards GRB 120815A at  $z = 2.36$ . *A&A***557** (2013) A18
- [15] D’Elia, V., Fynbo, J.P.U., Goldoni, P., Covino, S., de Ugarte Postigo, A., Ledoux, C., Calura, F., Gorosabel, J., Malesani, D., Matteucci, F., Sánchez-Ramírez, R., Savaglio, S., Castro-Tirado, A.J., Hartoog, O.E., Kaper, L., Muñoz-Darias, T., Pian, E., Piranomonte, S., Tagliaferri, G., Tanvir, N., Vergani, S.D., Watson, D.J., Xu, D.: VLT/X-shooter spectroscopy of the GRB 120327A afterglow. *A&A***564** (2014) A38
- [16] Friis, M., De Cia, A., Kruhler, T., Fynbo, J.P.U., Ledoux, C., Vreeswijk, P.M., Watson, D.J., Malesani, D., Gorosabel, J., Starling, R.L.C., Jakobsson, P., Varela, K., Wiersema, K., Drachmann, A.P., Trotter, A., Thone, C.C., de Ugarte Postigo, A., D’Elia, V., Elliott, J., Maturi, M., Goldoni, P., Greiner, J., Haislip, J., Kaper, L., Knust, F., LaCluyze, A., Milvang-Jensen, B., Reichart, D., Schulze, S., Sudilovsky, V., Tanvir, N., Vergani, S.D.: The warm, the excited, and the molecular gas: GRB 121024A shining through its star-forming galaxy. *MNRAS***451** (2015) 167–183
- [17] Welty, D.E., Xue, R., Wong, T.: Interstellar H I and  $H_2$  in the Magellanic Clouds: An Expanded Sample Based on Ultraviolet Absorption-line Data. *ApJ***745** (2012) 173
- [18] Noterdaeme, P., Ledoux, C., Petitjean, P., Srianand, R.: Molecular hydrogen in high-redshift damped Lyman- $\alpha$  systems: the VLT/UVES database. *A&A***481** (2008) 327–336
- [19] Balashev, S.A., Klimenko, V.V., Ivanchik, A.V., Varshalovich, D.A., Petitjean, P., Noterdaeme, P.: Molecular hydrogen absorption systems in Sloan Digital Sky Survey. *MNRAS***440** (2014) 225–239
- [20] Jorgenson, R.A., Murphy, M.T., Thompson, R., Carswell, R.F.: The Magellan uniform survey of damped Lyman  $\alpha$  systems – II. Paucity of strong molecular hydrogen absorption. *MNRAS***443** (2014) 2783–2800
- [21] York, D.G., Adelman, J., Anderson, Jr., J.E., Anderson, S.F., Annis, J., Bahcall, N.A., Bakken, J.A., Barkhouser, R., Bastian, S., Berman, E., Boroski, W.N., Bracker, S., Briegel, C., Briggs, J.W., Brinkmann, J., Brunner, R., Burles, S., Carey, L., Carr, M.A., Castander, F.J., Chen, B., Colestock, P.L., Connolly, A.J., Crocker, J.H., Csabai, I., Czarapata, P.C., Davis, J.E., Doi, M., Dombeck, T., Eisenstein, D., Ellman, N., Elms, B.R., Evans, M.L., Fan, X., Federwitz, G.R., Fiscelli, L., Friedman, S., Frieman, J.A., Fukugita, M., Gillespie, B., Gunn, J.E., Gurbani, V.K., de Haas, E., Haldeman, M., Harris, F.H., Hayes, J., Heckman, T.M., Hennessy, G.S., Hindsley, R.B., Holm, S., Holmgren, D.J., Huang, C.h., Hull, C., Husby, D., Ichikawa, S.I., Ichikawa, T., Ivezić, Z., Kent, S., Kim, R.S.J., Kinney, E., Klaene, M., Kleinman, A.N., Kleinman, S., Knapp, G.R., Korienek, J., Kron, R.G., Kunszt, P.Z., Lamb, D.Q., Lee, B., Leger, R.F., Limmongkol, S., Lindenmeyer, C., Long, D.C., Loomis, C., Loveday, J., Lucinio, R., Lupton, R.H., MacKinnon, B., Mannery, E.J., Mantsch, P.M., Margon, B., McGehee, P., McKay, T.A., Meiksin, A., Merelli, A., Monet, D.G., Munn, J.A., Narayanan, V.K., Nash, T., Neilsen, E., Neswold, R., Newberg, H.J., Nichol, R.C., Nicinski, T., Nonino, M., Okada, N., Okamura, S., Ostriker, J.P., Owen, R., Pauls, A.G., Peoples, J., Peterson, R.L., Petravick, D., Pier, J.R., Pope, A., Pordes, R., Prosapio, A., Rechenmacher, R., Quinn, T.R., Richards, G.T., Richmond, M.W., Rivetta, C.H., Rockosi, C.M., Ruthmansdorfer, K., Sandford, D., Schlegel, D.J., Schneider, D.P., Sekiguchi, M., Sergey, G., Shimasaku, K., Siegmund, W.A., Smee, S., Smith, J.A., Snedden, S., Stone, R., Stoughton, C., Strauss, M.A., Stubbs, C., SubbaRao, M., Szalay, A.S., Szapudi, I., Szokoly, G.P., Thakar, A.R., Tremonti, C., Tucker, D.L., Uomoto, A., Vanden Berk, D., Vogeley, M.S., Waddell, P., Wang, S.i., Watanabe, M., Weinberg, D.H., Yanny, B., Yasuda, N., SDSS Collaboration: The Sloan Digital Sky Survey: Technical Summary. *AJ***120** (2000) 1579–1587
- [22] Malec, A.L., Buning, R., Murphy, M.T., Milutinovic, N., Ellison, S.L., Prochaska, J.X., Kaper, L., Tumlinson, J., Carswell, R.F., Ubachs, W.: Keck telescope constraint on cosmological variation of the proton-to-electron mass ratio. *MNRAS***403** (2010) 1541–1555
- [23] Tumlinson, J., Malec, A.L., Carswell, R.F., Murphy, M.T., Buning, R., Milutinovic, N., Ellison, S.L., Prochaska, J.X., Jorgenson, R.A., Ubachs, W., Wolfe, A.M.: Cosmological Concordance or Chemical Coincidence? Deuterated Molecular Hydrogen Abundances at High Redshift. *ApJ***718** (2010) L156–L160
- [24] Som, D., Kulkarni, V.P., Meiring, J., York, D.G., Péroux, C., Khare, P., Lauroesch, J.T.: Element abundances at high redshift: MIKE observations of sub-damped Lyman  $\alpha$  absorbers at  $1.7 < z < 2.4$ . *MNRAS***435** (2013) 1469–1485
- [25] Jura, M.: Chlorine-Bearing Molecules in Interstellar Clouds. *ApJ***190** (1974) L33
- [26] Noterdaeme, P., Petitjean, P., Srianand, R., Ledoux, C., Le Petit, F.: Physical conditions in the neutral interstellar medium at  $z = 2.43$  toward Q 2348–011. *A&A***469** (2007) 425–436
- [27] Balashev, S.A., Noterdaeme, P., Klimenko, V.V., Petitjean, P., Srianand, R., Ledoux, C., Ivanchik, A.V., Varshalovich, D.A.: Neutral chlorine and molecular hydrogen at high redshift. *A&A***575** (2015) L8
- [28] van Weerdenburg, F., Murphy, M.T., Malec, A.L., Kaper, L., Ubachs, W.: First Constraint on Cosmological Variation of the Proton-to-Electron Mass Ratio from Two Independent Telescopes. *Physical Review Letters* **106** (2011) 180802
- [29] Noterdaeme, P., Ledoux, C., Petitjean, P., Le Petit, F., Srianand, R., Smette, A.: Excitation mechanisms in newly discovered  $H_2$ -bearing damped Lyman- $\alpha$  clouds: systems with low molecular fractions. *A&A***474** (2007) 393–407
- [30] Ivanchik, A.V., Petitjean, P., Balashev, S.A., Srianand, R., Varshalovich, D.A., Ledoux, C., Noterdaeme, P.: HD molecules at high redshift: the absorption system at  $z = 2.3377$  towards Q 1232 + 082. *MNRAS***404** (2010) 1583–1590
- [31] Albornoz Vázquez, D., Rahmani, H., Noterdaeme, P., Petitjean, P., Srianand, R., Ledoux, C.: Molecular hydrogen in the  $z_{abs} = 2.66$  damped Lyman- $\alpha$  absorber towards Q J 0643–5041. Physical conditions and limits on the cosmological variation of the proton-to-electron mass ratio. *A&A***562**

- (2014) A88
- [32] Balashev, S.A., Varshalovich, D.A., Ivanchik, A.V.: Directional radiation and photodissociation regions in molecular hydrogen clouds. *Astronomy Letters* **35** (2009) 150–166
- [33] Balashev, S.A., Petitjean, P., Ivanchik, A.V., Ledoux, C., Srianand, R., Noterdaeme, P., Varshalovich, D.A.: Partial coverage of the broad-line region of Q1232+082 by an intervening H<sub>2</sub>-bearing cloud. *MNRAS* **418** (2011) 357–369
- [34] Klimenko, V.V., Balashev, S.A., Ivanchik, A.V., Ledoux, C., Noterdaeme, P., Petitjean, P., Srianand, R., Varshalovich, D.A.: Partial covering of the emission regions of Q 0528-250 by intervening H<sub>2</sub> clouds. *MNRAS* **448** (2015) 280–298
- [35] Ofengeim, D.D., Balashev, S.A., Ivanchik, A.V., Kaminker, A.D., Klimenko, V.V.: Effect of a partial coverage of quasar broad-line regions by intervening H<sub>2</sub>-bearing clouds. *Ap&SS* **359** (2015) 26
- [36] Sugiura, N.: "Further analysis of the data by Akaike's information criterion and the finite corrections. *Commun. Stat. A-Theor.* **7** (1978) 13–26
- [37] Liddle, A.R.: Information criteria for astrophysical model selection. *MNRAS* **377** (2007) L74–L78
- [38] Ivanov, T.I., Dickenson, G.D., Roudjane, M., Oliveira, N.D., Joyeux, D., Nahon, L., Tchang-Brillet, W.U.L., Ubachs, W.: Fourier-transform spectroscopy of HD in the vacuum ultraviolet at  $\lambda = 87$ –112 nm. *Molecular Physics* **108** (2010) 771–786
- [39] Abgrall, H., Roueff, E.: Theoretical calculations of excited rovibrational levels of HD. Term values and transition probabilities of VUV electronic bands. *A&A* **445** (2006) 361–372
- [40] Dalgarno, A., Lepp, S.: Deuterium fractionation mechanisms in interstellar clouds. *ApJ* **287** (1984) L47–L50
- [41] Welty, D.E., Hobbs, L.M., Morton, D.C.: High-Resolution Observations of Interstellar Ca I Absorption-Implications for Depletions and Electron Densities in Diffuse Clouds. *ApJS* **147** (2003) 61–96
- [42] Nahar, S.N., Pradhan, A.K.: Electron-Ion Recombination Rate Coefficients, Photoionization Cross Sections, and Ionization Fractions for Astrophysically Abundant Elements. I. Carbon and Nitrogen. *ApJS* **111** (1997) 339–355
- [43] Le Petit, F., Roueff, E., Le Bourlot, J.: D/HD transition in Photon Dominated Regions (PDR). *A&A* **390** (2002) 369–381
- [44] Habing, H.J.: The interstellar radiation density between 912 Å and 2400 Å. *Bull. Astron. Inst. Netherlands* **19** (1968) 421
- [45] Planck Collaboration, Ade, P.A.R., Aghanim, N., Arnaud, M., Ashdown, M., Aumont, J., Baccigalupi, C., Banday, A.J., Barreiro, R.B., Bartlett, J.G., et al.: Planck 2015 results. XIII. Cosmological parameters. *ArXiv e-prints* (2015)
- [46] Lacour, S., André, M.K., Sonnentrucker, P., Le Petit, F., Welty, D.E., Desert, J.M., Ferlet, R., Roueff, E., York, D.G.: Deuterated molecular hydrogen in the Galactic ISM. New observations along seven translucent sightlines. *A&A* **430** (2005) 967–977
- [47] Balashev, S.A., Ivanchik, A.V., Varshalovich, D.A.: HD/H<sub>2</sub> molecular clouds in the early Universe: The problem of primordial deuterium. *Astronomy Letters* **36** (2010) 761–772
- [48] Black, J.H., Dalgarno, A.: Interstellar H<sub>2</sub> - The population of excited rotational states and the infrared response to ultraviolet radiation. *ApJ* **203** (1976) 132–142
- [49] Jura, M.: Interstellar clouds containing optically thick H<sub>2</sub>. *ApJ* **197** (1975) 581–586
- [50] Jura, M.: Interstellar clouds containing optically thin H<sub>2</sub>. *ApJ* **197** (1975) 575–580
- [51] Abgrall, H., Le Bourlot, J., Pineau Des Forets, G., Roueff, E., Flower, D.R., Heck, L.: Photodissociation of H<sub>2</sub> and the H/H<sub>2</sub> transition in interstellar clouds. *A&A* **253** (1992) 525–536
- [52] Le Petit, F., Nehmé, C., Le Bourlot, J., Roueff, E.: A Model for Atomic and Molecular Interstellar Gas: The Meudon PDR Code. *ApJS* **164** (2006) 506–529
- [53] Ferland, G.J., Porter, R.L., van Hoof, P.A.M., Williams, R.J.R., Abel, N.P., Lykins, M.L., Shaw, G., Henney, W.J., Stancil, P.C.: The 2013 Release of Cloudy. *Rev. Mexicana Astron. Astrofis.* **49** (2013) 137–163
- [54] Spitzer, L.: Physical processes in the interstellar medium. (1978)
- [55] Forrey, R.C., Balakrishnan, N., Dalgarno, A., Lepp, S.: Quantum Mechanical Calculations of Rotational Transitions in H-H<sub>2</sub> Collisions. *ApJ* **489** (1997) 1000–1003
- [56] Abel, T., Anninos, P., Zhang, Y., Norman, M.L.: Modeling primordial gas in numerical cosmology. *New A* **2** (1997) 181–207
- [57] Draine, B.T., Bertoldi, F.: Structure of Stationary Photodissociation Fronts. *ApJ* **468** (1996) 269
- [58] Hirashita, H., Ferrara, A.: Molecular hydrogen in damped Ly $\alpha$  systems: clues to interstellar physics at high redshift. *MNRAS* **356** (2005) 1529–1541
- [59] Silva, A.I., Viegas, S.M.: Physical conditions in quasi-stellar object absorbers from fine-structure absorption lines. *MNRAS* **329** (2002) 135–148
- [60] Abrahamsson, E., Krems, R.V., Dalgarno, A.: Fine-Structure Excitation of O I and C I by Impact with Atomic Hydrogen. *ApJ* **654** (2007) 1171–1174
- [61] Schroder, K., Staemmler, V., Smith, M.D., Flower, D.R., Jaquet, R.: Excitation of the fine-structure transitions of C in collisions with ortho- and para-H<sub>2</sub>. *Journal of Physics B Atomic Molecular Physics* **24** (1991) 2487–2502
- [62] Staemmler, V., Flower, D.R.: Excitation of the C(2p<sup>2</sup> <sup>3</sup>P<sub>j</sub>) fine structure states in collisions with He(1s<sup>2</sup> <sup>1</sup>S<sub>0</sub>). *Journal of Physics B Atomic Molecular Physics* **24** (1991) 2343–2351
- [63] Steigman, G.: Primordial Nucleosynthesis in the Precision Cosmology Era. *Annual Review of Nuclear and Particle Science* **57** (2007) 463–491
- [64] Gry, C., Boulanger, F., Nehmé, C., Pineau des Forêts, G., Habart, E., Falgarone, E.: H<sub>2</sub> formation and excitation in the diffuse interstellar medium. *A&A* **391** (2002) 675–680
- [65] Ledoux, C., Noterdaeme, P., Petitjean, P., Srianand, R.: Neutral atomic-carbon quasar absorption-line systems at  $z > 1.5$ . Sample selection, H I content, reddening, and 2175 Å extinction feature. *A&A* **580** (2015) A8
- [66] Wolfire, M.G., Tielens, A.G.G.M., Hollenbach, D., Kaufman, M.J.: Chemical Rates on Small Grains and PAHs: C<sup>+</sup> Recombination and H<sub>2</sub> Formation. *ApJ* **680** (2008) 384–397
- [67] Liszt, H.S.: How does C<sup>+</sup> recombine in diffuse molecular gas? *A&A* **527** (2011) A45
- [68] Mathis, J.S., Mezger, P.G., Panagia, N.: Interstellar radiation field and dust temperatures in the diffuse interstellar matter and in giant molecular clouds. *A&A* **128** (1983) 212–229
- [69] Hollenbach, D., Kaufman, M.J., Neufeld, D., Wolfire, M., Goicoechea, J.R.: The Chemistry of Interstellar OH<sup>+</sup>, H<sub>2</sub>O<sup>+</sup>, and H<sub>3</sub>O<sup>+</sup>: Inferring the Cosmic-Ray Ionization Rates from Observations of Molecular Ions. *ApJ* **754** (2012) 105
- [70] Wright, E.L., Mather, J.C., Bennett, C.L., Cheng, E.S., Shafer, R.A., Fixsen, D.J., Eplee, Jr., R.E., Isaacman, R.B., Read, S.M., Boggess, N.W., Gulkis, S., Hauser, M.G., Janssen, M., Kelsall, T., Lubin, P.M., Meyer, S.S., Moseley, Jr., S.H., Murdock, T.L., Silverberg, R.F., Smoot, G.F., Weiss, R., Wilkinson, D.T.: Preliminary spectral observations of the Galaxy with a 7 deg beam by the Cosmic Background Explorer (COBE). *ApJ* **381** (1991) 200–209
- [71] Asplund, M., Grevesse, N., Sauval, A.J., Scott, P.: The Chemical Composition of the Sun. *ARA&A* **47** (2009) 481–522
- [72] Mathis, J.S., Rumpl, W., Nordsieck, K.H.: The size distribution of interstellar grains. *ApJ* **217** (1977) 425–433
- [73] Noterdaeme, P., Ledoux, C., Srianand, R., Petitjean, P., Lopez, S.: Diffuse molecular gas at high redshift. Detection of CO molecules and the 2175 Å dust feature at  $z = 1.64$ . *A&A* **503** (2009) 765–770
- [74] Bohlin, R.C., Savage, B.D., Drake, J.F.: A survey of interstellar H I from L-alpha absorption measurements. II. *ApJ* **224** (1978) 132–142
- [75] Le Bourlot, J., Le Petit, F., Pinto, C., Roueff, E., Roy, F.: Surface chemistry in the interstellar medium. I. H<sub>2</sub> formation by Langmuir-Hinshelwood and Eley-Rideal mechanisms. *A&A* **541** (2012) A76
- [76] Joulain, K., Falgarone, E., Pineau des Forets, G., Flower, D.: Non-equilibrium chemistry in the dissipative structures of interstellar turbulence. *A&A* **340** (1998) 241–256
- [77] Cecchi-Pestellini, C., Casu, S., Dalgarno, A.: H<sub>2</sub> excitation in turbulent interstellar clouds. *MNRAS* **364** (2005) 1309–1314
- [78] Le Petit, F., Roueff, E., Herbst, E.: H<sub>3</sub><sup>+</sup> and other species in the diffuse cloud towards  $\zeta$  Persei: A new detailed model. *A&A* **417** (2004) 993–1002
- [79] Haardt, F., Madau, P.: Radiative Transfer in a Clumpy Universe. II. The Ultraviolet Extragalactic Background. *ApJ* **461** (1996) 20
- [80] Liszt, H.S.: HD/H<sub>2</sub> as a Probe of the Roles of Gas, Dust,

Light, Metallicity, and Cosmic Rays in Promoting the Growth  
of Molecular Hydrogen in the Diffuse Interstellar Medium.  
ApJ**799** (2015) 66



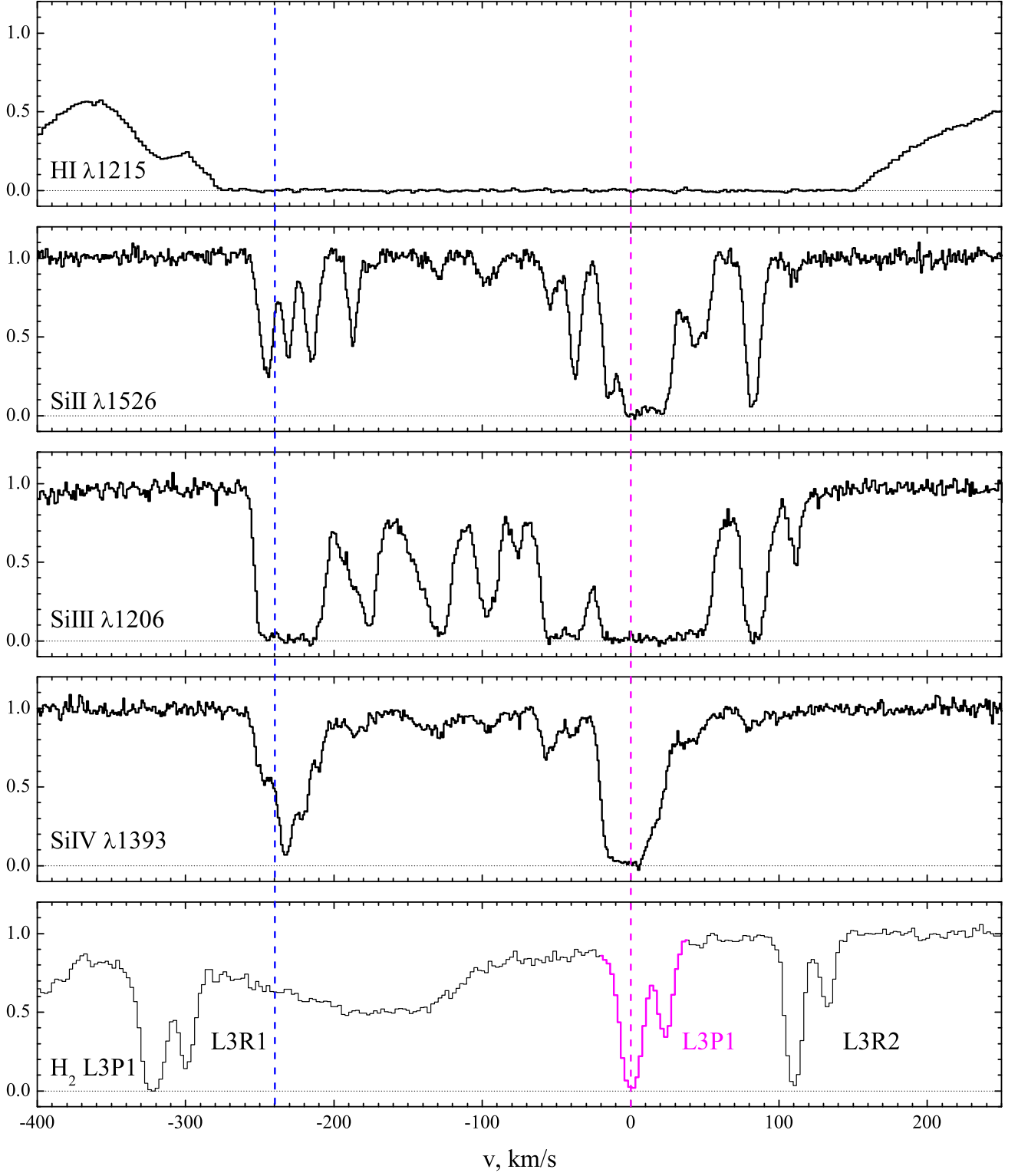


**Figure 2.** H I ( $\text{Ly}\alpha$ ), Si II, Si III, Si IV, and H<sub>2</sub> absorption line profiles. The dashed vertical lines indicate the positions of the two components of the sub-DLA system at  $z = 2.05684$  and  $2.05930$ . The lower panel shows the H<sub>2</sub> L3P1 line profile. The two components of the H<sub>2</sub> absorption system corresponding to the component of the sub-DLA system at  $z = 2.05930$  are highlighted by the thick line. The H<sub>2</sub> lines corresponding to the L3R1 and L3R2 transitions are also specified.

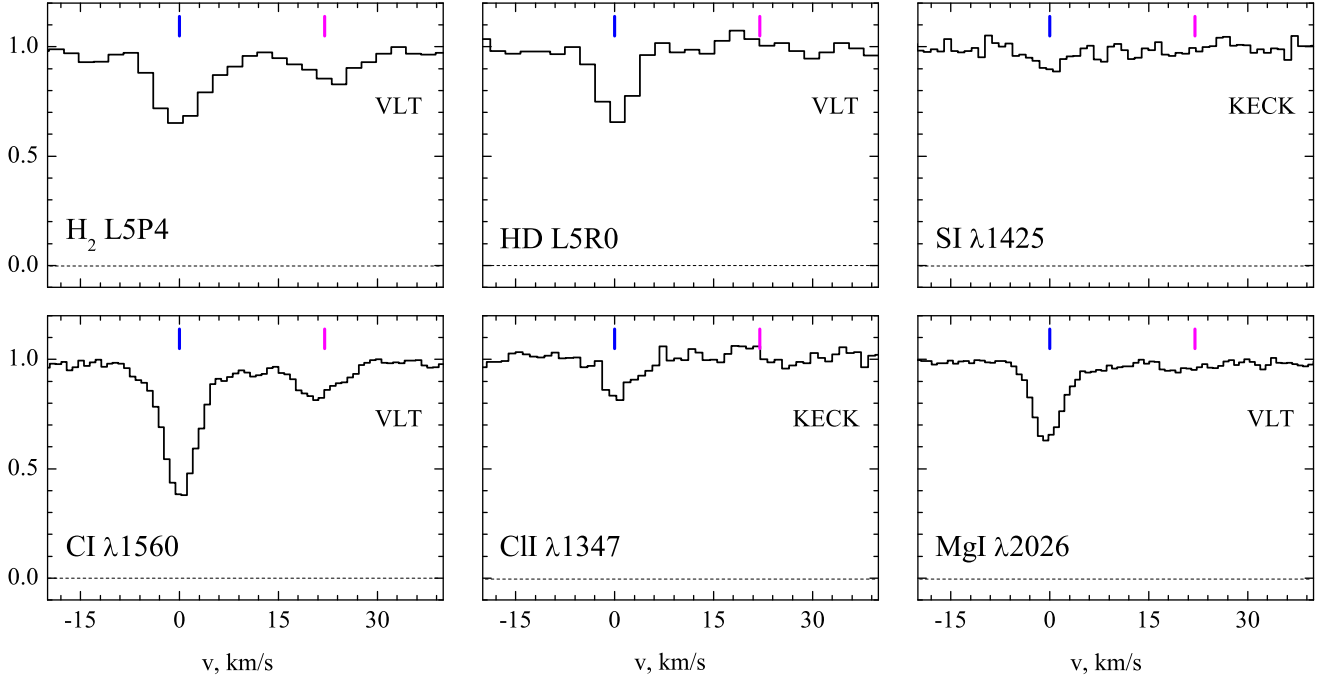


**Figure 3.** Absorption lines of neutral species associated with the H<sub>2</sub> system at  $z_{\text{abs}} = 2.059$  in the VLT/UVES and Keck/HIRES spectra of the quasar J 2123–0050. The vertical dashes indicate the positions of the two components of the H<sub>2</sub> absorption system (A and B) at redshifts  $z_{\text{abs}} = 2.05933$  and  $2.05955$ . Only the C I lines are detected at the redshift of component B. The velocity shift shown along the horizontal axis is calculated relative to component A.

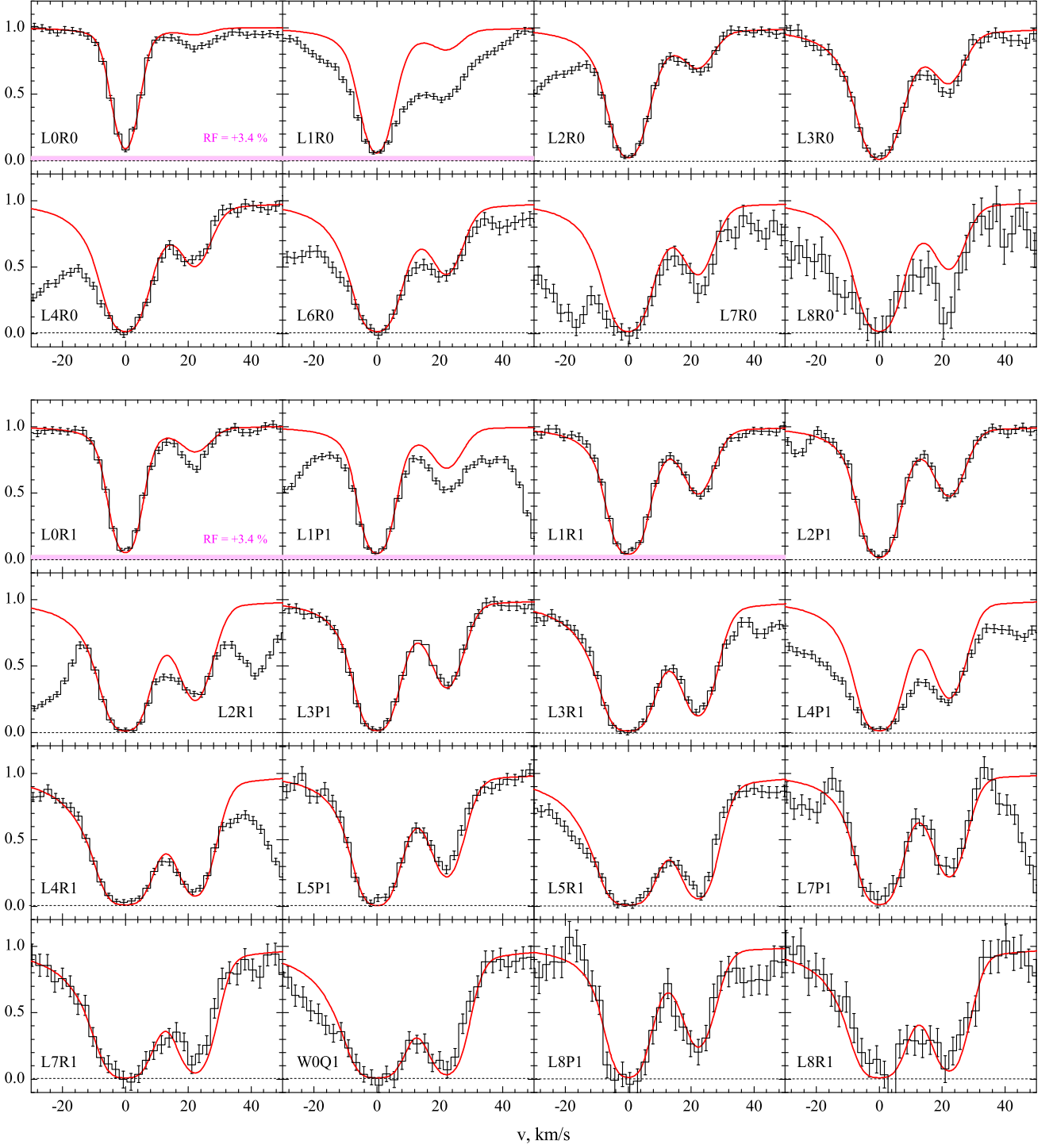


**Figure 4.** Synthetic spectrum of the  $\text{H}_2$  system at  $z_{\text{abs}} = 2.059$  in the spectrum of the quasar J2123–0050 (VLT/UVES). The lines of the transitions in the  $\text{H}_2$  absorption system from the rotational  $J = 0, 1$  levels are shown. The synthetic spectrum was corrected for the coverage factor (see Section 4.2). The velocity shift shown along the horizontal axis is calculated relative to component A.

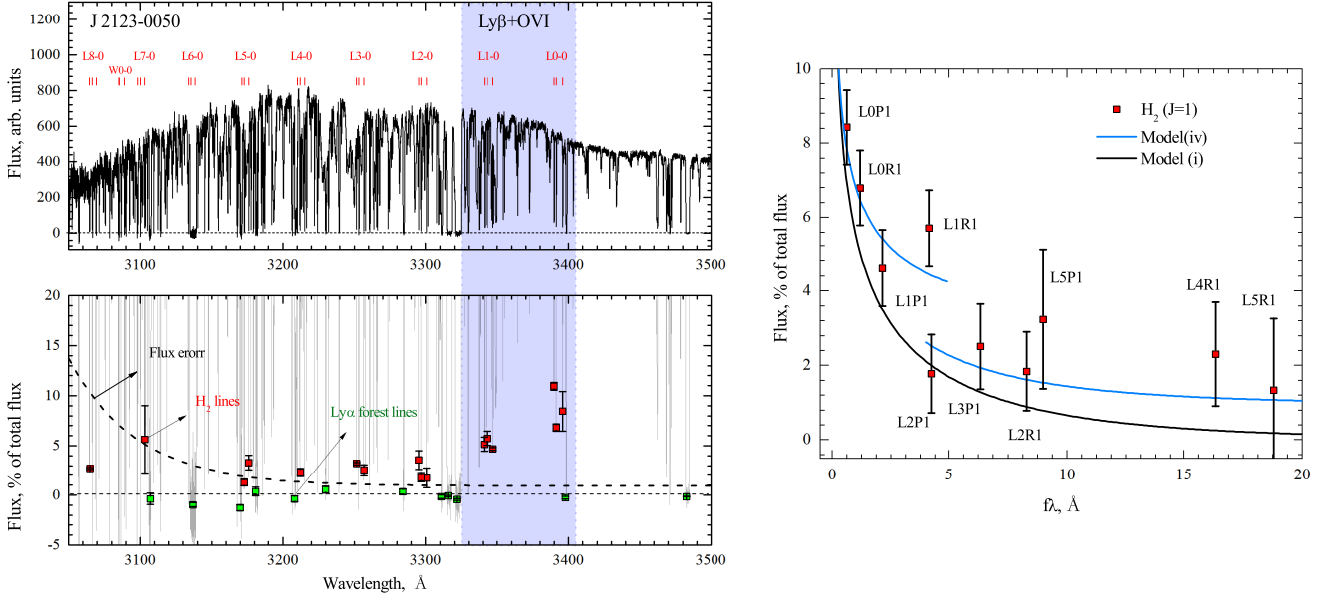


**Figure 6.** The left panels show the region of the VLT/EVES spectrum for the quasar J 2123.0050 containing the H<sub>2</sub> absorption lines. On the upper left panel, the observed flux from the quasar in arbitrary units is shown along the vertical axis; the normalized flux in % of the total flux is shown on the lower left panel. The gray color highlights the region of the spectrum containing the quasar's Ly $\alpha$  and OVI emission lines. The open and black filled squares indicate the residual fluxes at the bottom of the H<sub>2</sub> and Ly $\alpha$ -forest lines, respectively. The dashed line indicates the statistical error of the flux in the spectrum. The right panel shows the residual fluxes in the H<sub>2</sub> lines of the transitions from the J = 1 level as a function of  $f\lambda$ , the product of the oscillator strength by the transition wavelength. The solid and dashed lines indicate the calculations performed for the models with and without allowance for the partial coverage effect, models (iv) and (i), respectively (see Table 3).

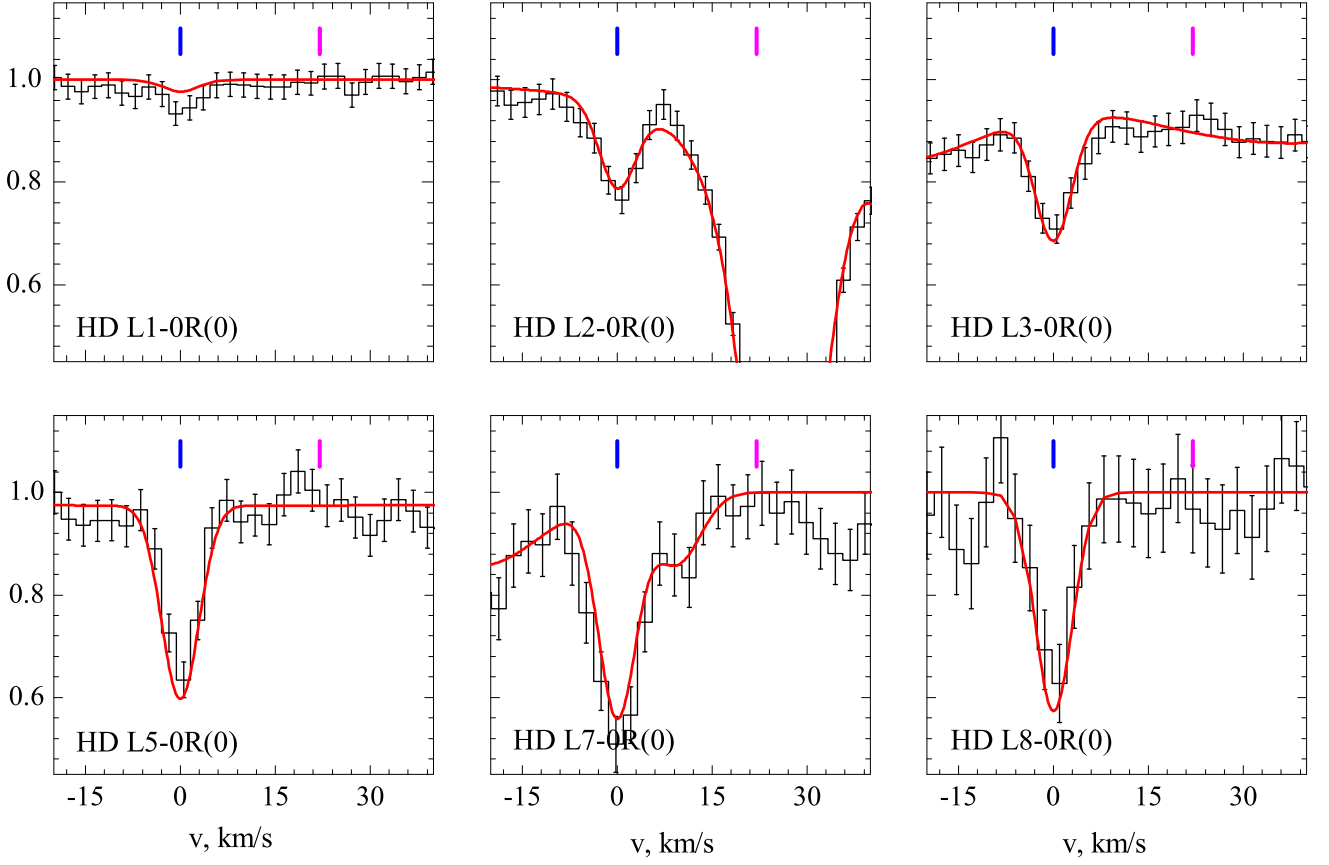


**Figure 7.** Synthetic spectrum of HD molecules at  $z_{\text{abs}} = 2.05933$  fitted into the observed spectrum of the quasar J2123–0050 (VLT/UVES). The vertical dashes indicate the positions of the two components of the  $H_2$  absorption system (A and B). The velocity shift shown along the horizontal axis is calculated relative to component A, in which the HD lines are detected.

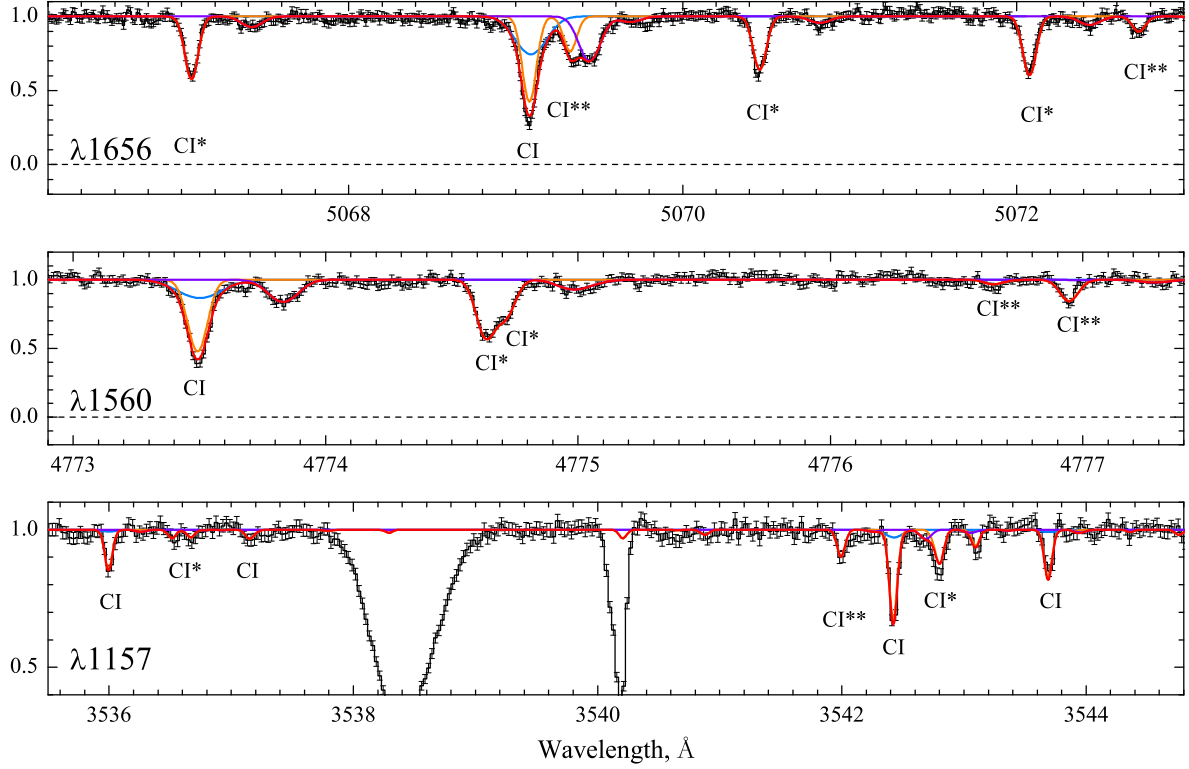


**Figure 8.** Synthetic spectrum of the C I lines associated with the H<sub>2</sub> absorption system fitted into the observed spectrum of the quasar J2123–0050 (UVES/VLT). The profiles of the individual C I line components are indicated by the thin solid lines.

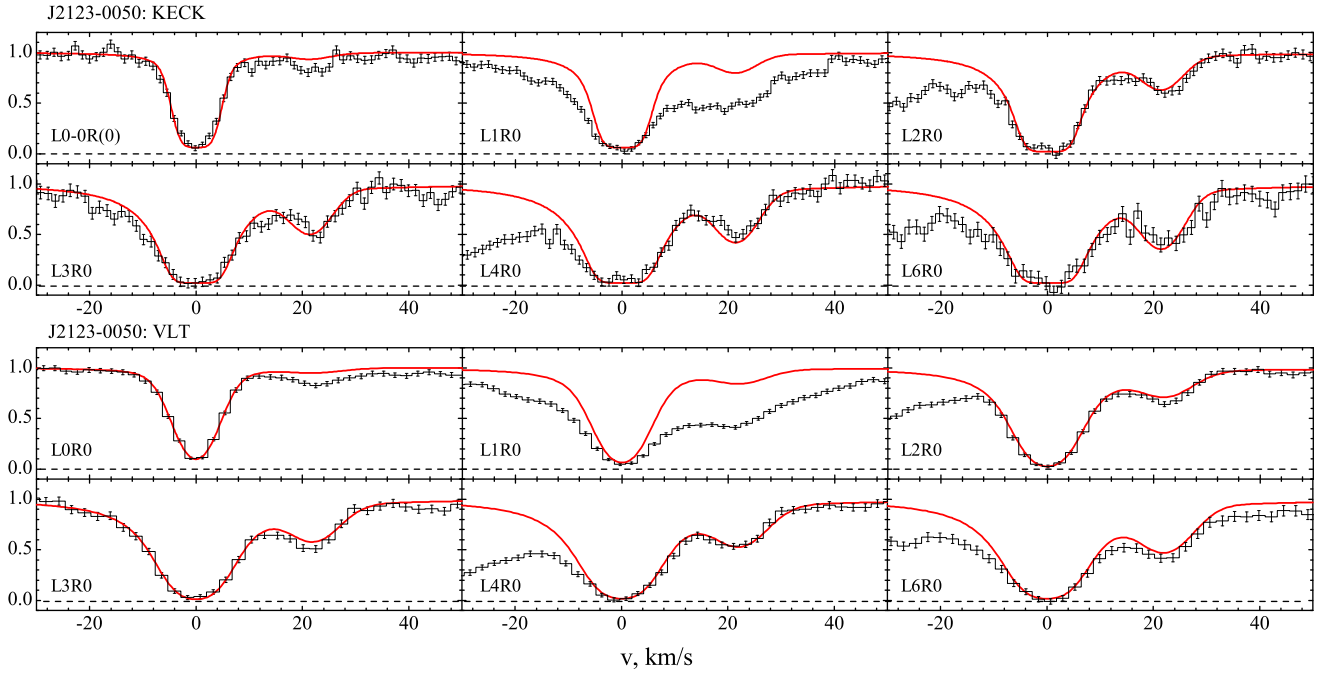


**Figure 9.** Synthetic spectrum of the H<sub>2</sub> lines of the transitions from the  $J = 0$  level fitted into the Keck/HIRES (upper panel) and VLT/UVES (lower panel) spectra of the quasar J2123–0050. The H<sub>2</sub> column density in component A was assumed to be  $\log N_{\text{H}_2}^{\text{A}}(J = 0) = 17.37$ . Since the widths of the HIRES/Keck ( $\sim 3$  km/s) and UVES/VLT ( $\sim 6$  km/s) point spread functions differ, the profiles of the corresponding H<sub>2</sub> lines on the upper and lower panels differ.

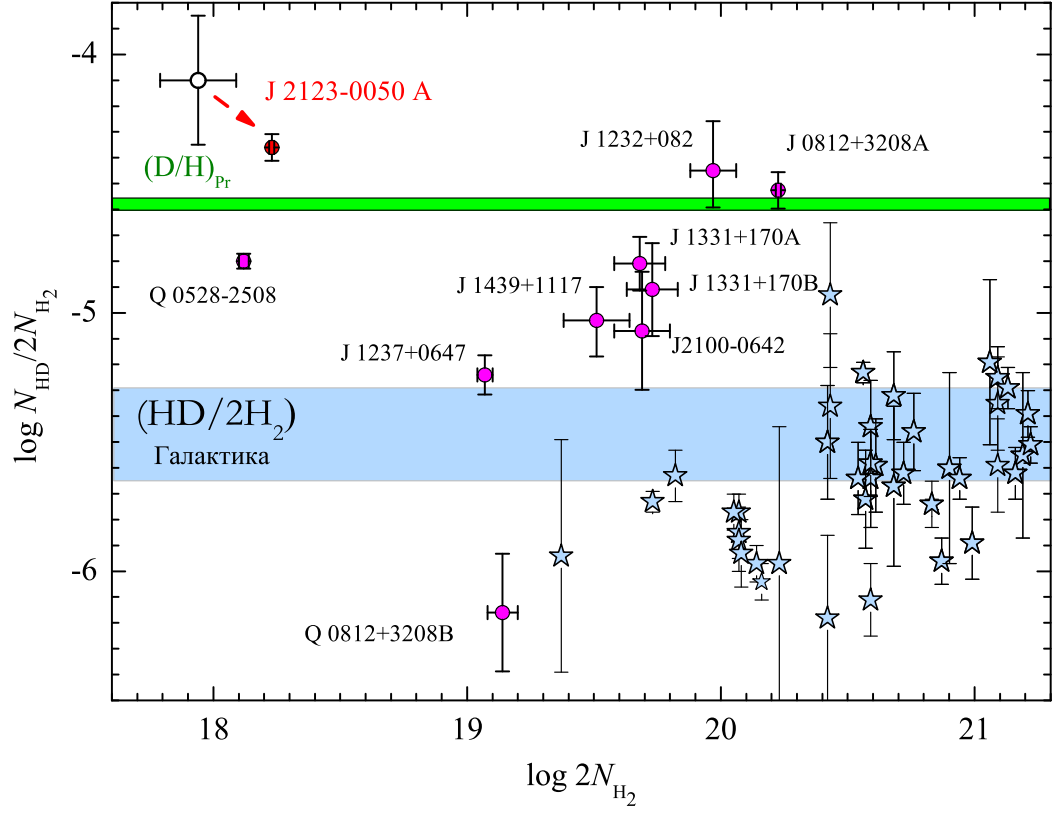


**Figure 10.** Measured  $N_{\text{HD}}/2N_{\text{H}_2}$  ratios for high-redshift absorption systems (filled circles) and for systems in our Galaxy (open stars). The solid horizontal line indicates the relative primordial deuterium abundance  $(\text{D}/\text{H})$  estimated by analyzing the CMBR anisotropy power spectrum [45]. The result of the  $\text{H}_2/\text{HD}$  system in the spectrum of J 2123–0050 presented in [23] is indicated by the open circle.

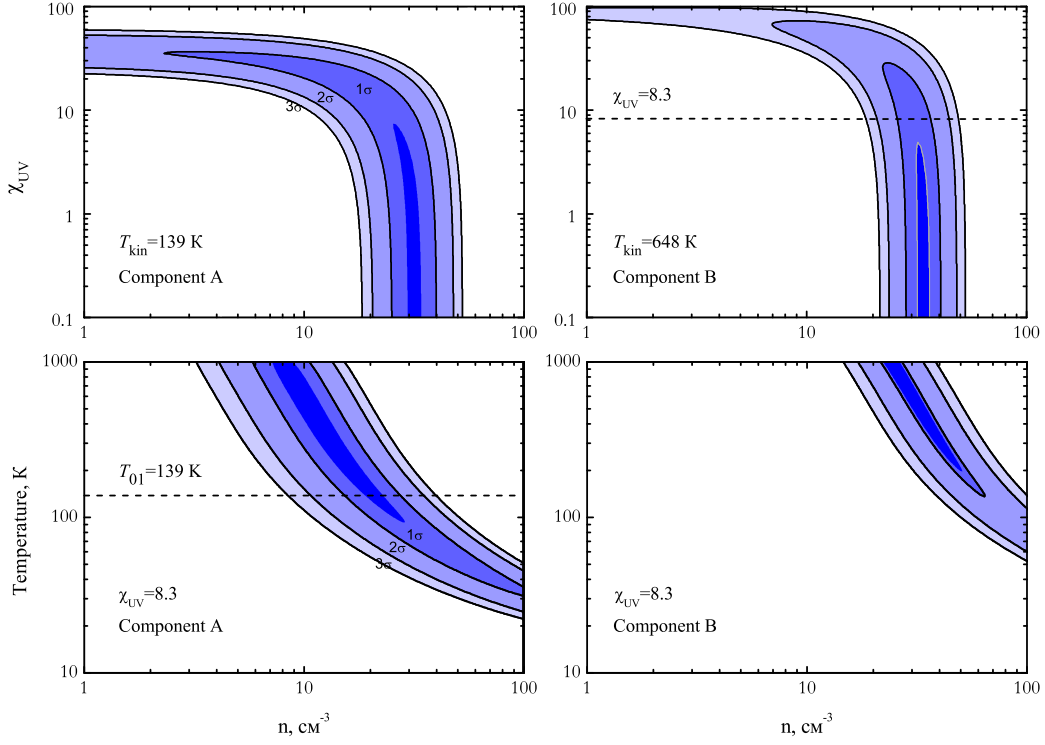


**Figure 11.** The 1, 2, and  $3\sigma$  confidence regions for determining the physical conditions by analyzing the C I fine-structure level populations for components A and B (the left and right panels, respectively). The upper panels show the confidence regions for the UV background intensity ( $\chi_{UV}$ , in units of the mean Galactic value) and the number density. The temperature was assumed to be equal to the value determined from the ortho-to-para-hydrogen ratio, 139 and 648 K for components A and B, respectively. The lower panels show the confidence regions for the temperature and the number density. The UV background intensity was assumed to be higher than the mean Galactic value by a factor of 8.3.



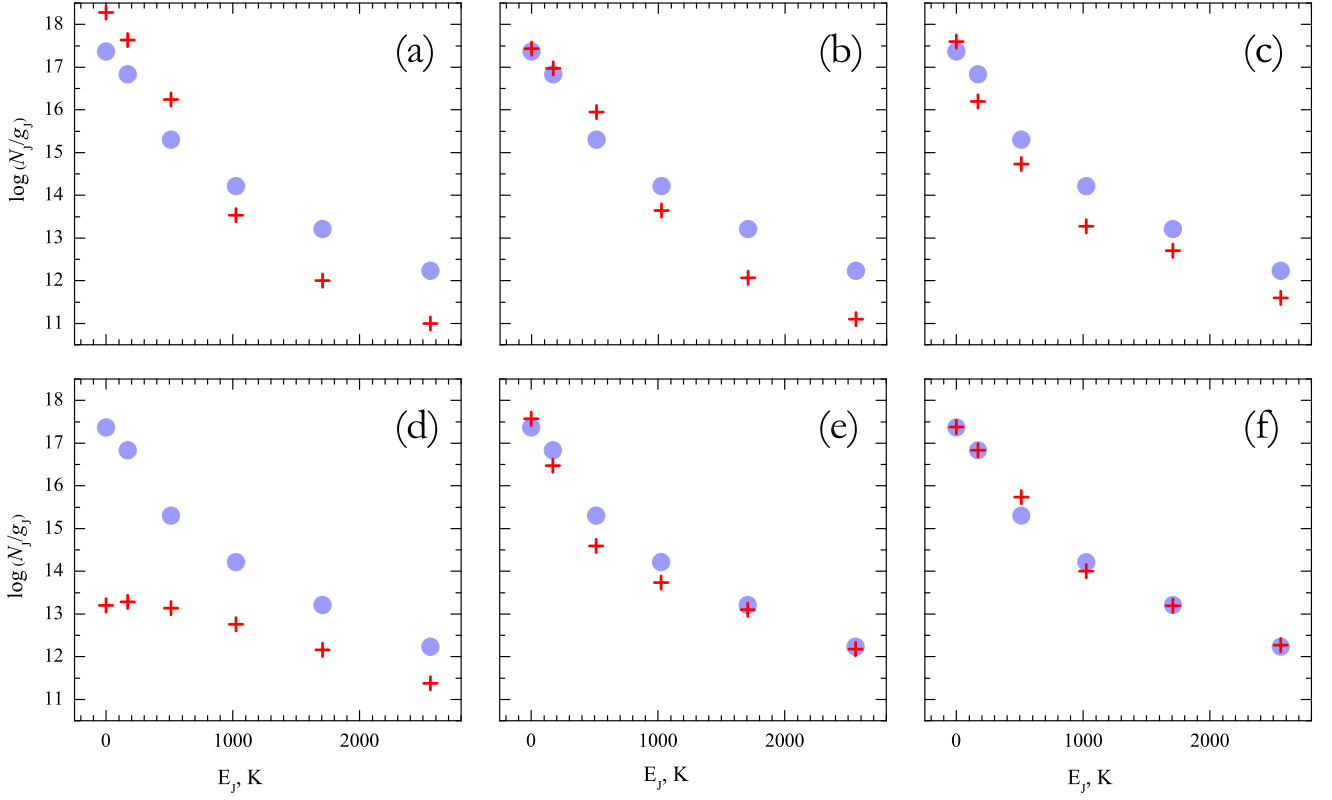


**Figure 12.** Comparison of the measured H<sub>2</sub> level populations for component A (gray circles) with the results of our PDR Meudon simulations (red crosses) for six models (a)  $\tilde{U}$ –(f), whose parameters are given in Table 5.

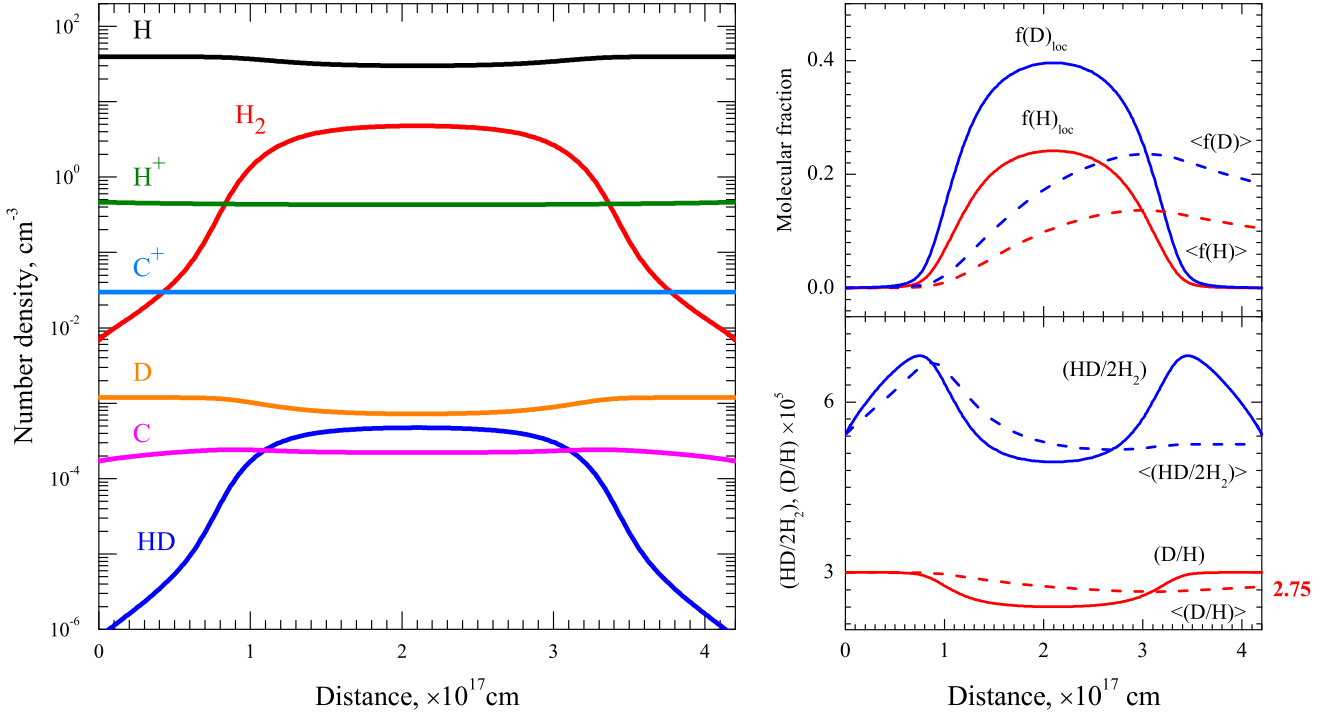


**Figure 13.** Structure of the molecular cloud obtained in the PDR Meudon model (model (f), see Table 5). The left panel shows the number density profiles for the species in the cloud. The solid and dashed lines on the right panels indicate the dependences of the absolute and mean H and D molecular fractions (upper panel) as well as the  $N_{HD}/2N_{H_2}$  and  $N_D/N_H$  ratios (lower panel). The averaging was performed from one of the cloud boundaries.

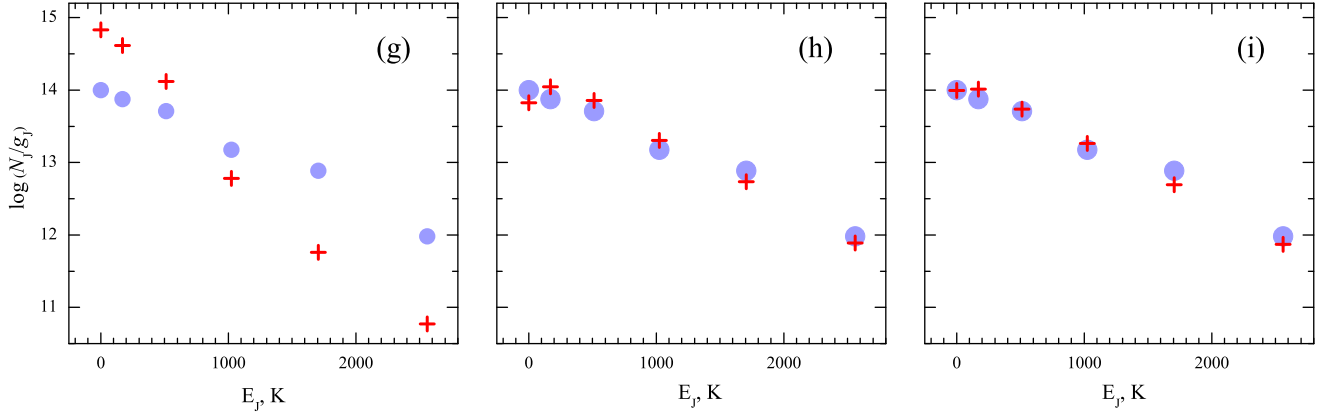


**Figure 14.** Comparison of the measured  $H_2$  level populations for component B (gray circles) with the results of our PDR Meudon simulations (red crosses) for three models (g)–(i), whose parameters are given in Table 6.

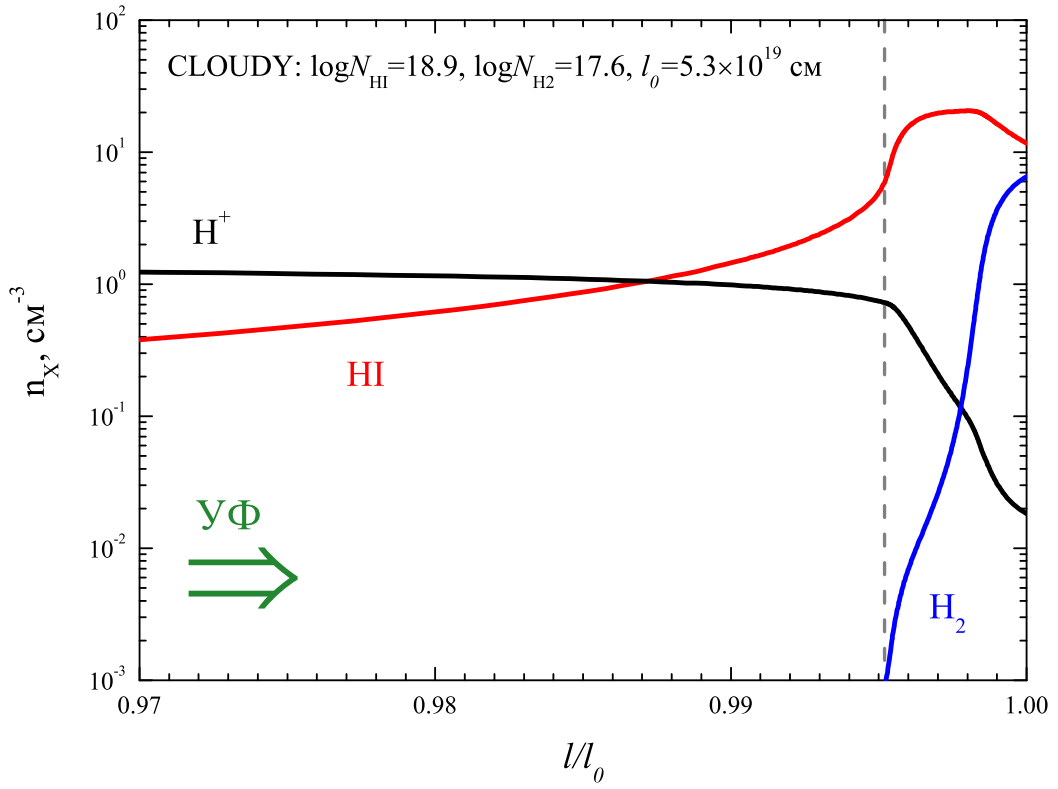


**Figure 15.** Results of our simulations of the structure of the sub-DLA system with the CLOUDY code. The dependences of the  $H^+$ ,  $HI$ , and  $H_2$  number densities on the distance from the boundary are shown. The calculations were performed in a plane-parallel model. The medium is irradiated by UV radiation only on the left side. The vertical line indicates an arbitrary boundary between the regions of hot ionized and cold neutral media.